Review

doi.org/10.1002/tcr.202200208
tcr.wiley-vch.de

THE CHEMICAL RECORD

Tetracyanobutadiene Bridged Push-Pull Chromophores: Development of New Generation Optoelectronic Materials

Yuvraj Patil,[a, c] Holger Butenschön,*[b] and Rajneesh Misra*[a]

Dedicated to the memory of Professor Dr. François Diederich.

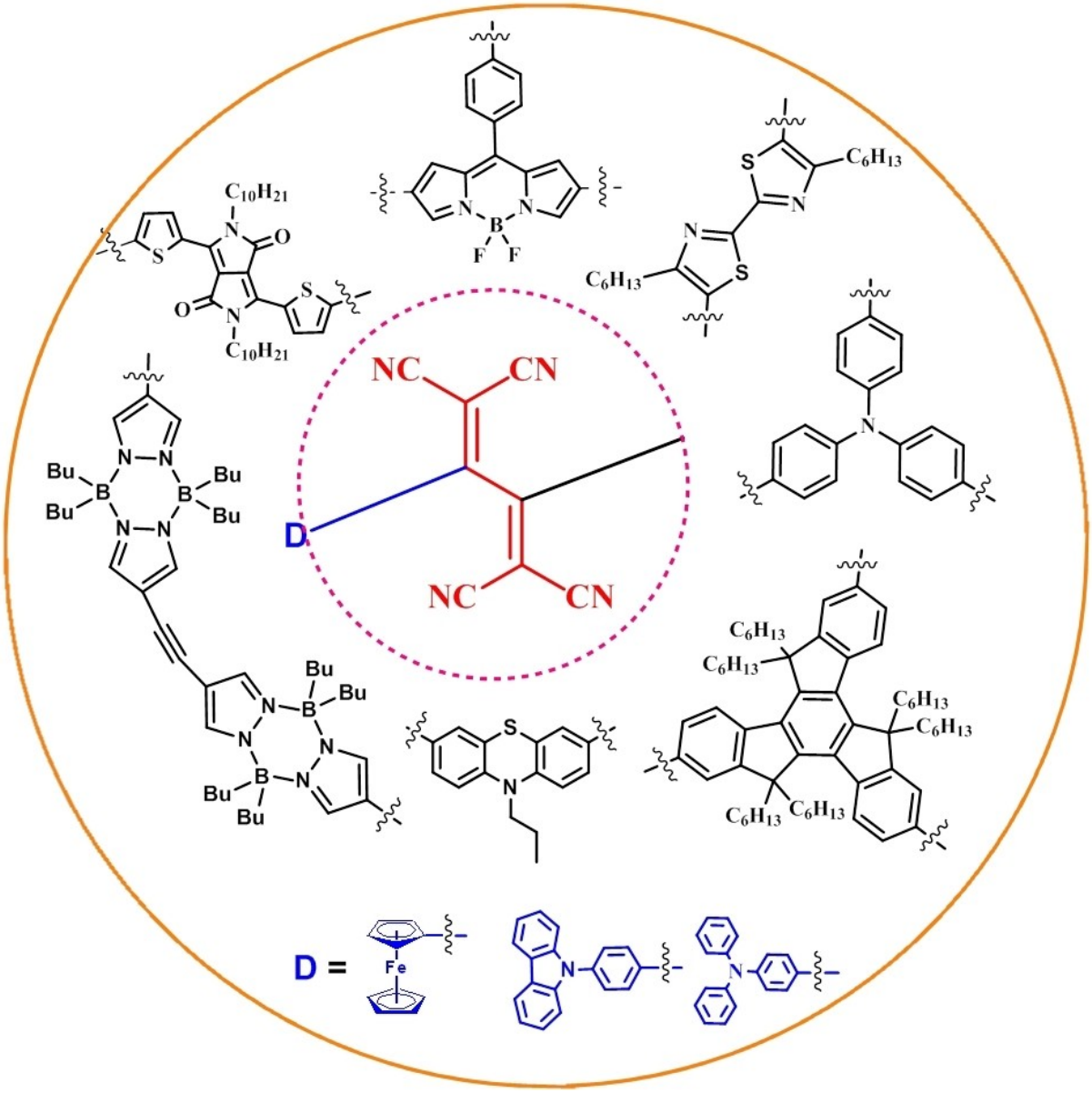

Abstract: This review describes the design strategies used for the synthesis of various tetracyanobutadiene bridged donor-acceptor molecular architectures by a click type [2+2] cycloaddition-retroelectrocyclization (CA-RE) reaction sequence. The photophysical and electrochemical properties of the tetracyanobutadiene bridged molecular architectures based on various moieties including diketopyrrolopyrrole, isoindigo, benzothiadiazole, pyrene, pyrazabole, truxene, boron dipyrromethene (BODIPY), phenothiazine, triphenylamine, thiazole and bisthiazole are summarized. Further, we discuss some important applications of the tetracyanobutadiene bridged derivatives in dye sensitized solar cells, bulk heterojunction solar cells and photothermal cancer therapy.

Keywords: Tetracyanoethylene, Cycloaddition-retroelectrocyclization, Solar Cells, Photothermal Therapy

1. Introduction

In recent years, tremendous growth has been observed in the development of donor-acceptor molecular systems for optoelectronic applications.[1,2] Small organic molecules containing π−bridged donor-acceptor (D-π-A) frameworks are of significant interest due to their broad absorption and low HOMO-LUMO gap.[3]

Tetracyanoethylene (TCNE) is a highly electron deficient organic compound consisting of four cyano groups attached to an ethylene moiety.[4] It possesses characteristic properties such as a strong electron withdrawing ability and is widely used for cycloaddition reactions. The click type [2+2] cycloaddition-retroelectrocyclization (CA-RE) reaction sequence of electron rich alkynes **1** with TCNE via cyclobutene intermediates **2** is generally a fast, atom-economic, catalyst free and high yielding reaction providing an efficient strategy widely used for the design of tetracyanobutadiene (TCBD) bridged donor-acceptor molecular architectures **3**.[4,5] Thus, often an improvement of the acceptor strength and non-planarity of the molecular structure can be achieved resulting in tunable charge-transfer interactions.[4] Recently, a number of TCBD derivatives has been reported in the literature, and some of them are used for organic solar cells.[6–12] The general reaction sequence is given in Scheme 1.[13]

To the best of our knowledge this reaction was first reported by Bruce *et al.* for metal-acetylide complexes in 1981.[14] Diederich *et al.* explored various TCBD derivatives by CA-RE reaction sequences of donor substituted alkynes with TCNE.[5,15,18a] The nature and number of substituents attached to the alkyne significantly affect the reactivity towards TCNE as well as the reaction yield. The beauty of CA-RE reaction is that it results in high yield without formation of by-products.

In this review we discuss the design strategies used for the synthesis of TCBD bridged molecular architectures based on various chromophores including diketopyrrolopyrrole, isoindigo, benzothiadiazole, pyrene, pyrazabole, truxene, boron dipyrromethene (BODIPY), phenothiazine, triphenylamine thiazole and bisthiazole. Further, some important applications of TCBD derivatives in solar cells and photothermal cancer therapy are discussed.

1.1. Triphenylamine Based TCBD Derivatives

Triphenylamine and ferrocene are well known electron donors, their alkyne substituted derivatives undergo CA-RE reaction[17–28] with TCNE. Triphenylamine and ferrocene based molecular systems are widely used for various technological applications in organic field effect transistors (OFETs) and organic solar cells (OSCs).[29,30] Ferrocene derivatives usually give one reversible low oxidation potential wave in the cyclic voltammogram and exhibit a strong nonlinear optical (NLO) response.

Triphenylamine derivatives (**TPAs 1–3**) were synthesized by the CA-RE reaction of phenylethynyl substituted triphenylamine with one, two, and three equivalents of TCNE in 50–54% yield (Figure 1).[31] Their photophysical and electrochemical properties were reported which show strong intramolecular charge transfer (ICT) interactions (Figure 2). The mono-TCBD bridged triphenylamine derivative **TPA-1** with two phenylethynyl substituents shows its absorption maximum

[a] *Dr. Y. Patil, Prof. Dr. R. Misra*
Department of Chemistry, Indian Institute of Technology Indore, Indore 453552 (India)
E-mail: rajneeshmisra@iiti.ac.in
[b] *Prof. Dr. H. Butenschön*
Institut für Organische Chemie, Leibniz Universität Hannover, Schneiderberg 1B, 30167 Hannover, Germany
E-mail: holger.butenschoen@mbox.oci.uni-hannover.de
[c] *Dr. Y. Patil*
Present Address: Institut des Sciences Chimiques de Rennes (ISCR) – Université de Rennes 1, Rennes 35700, France

at 510 nm, and further incorporation of a second and a third TCBD unit blue shifts the absorption by 3 nm and 16 nm, respectively. As the number of TCBD units in the in **TPAs 1–3** increases, the electronic absorption spectra show a blue shift of the $\pi \rightarrow \pi^*$ transition band (300–400 nm) and the ICT band (400–700 nm). The electrochemical investigation showed that high oxidation and reduction potentials were observed as the number of TCBD unit's increases in the molecular architecture, which was further supported by computational calculation. DFT studies indicated that by increasing the number of TCBD units in the phenylethynyl substituted triphenylamine, the HOMO-LUMO gap increases from 2.32 eV in **TPA-1** to 2.42 eV in **TPA-2** to 2.79 eV in **TPA-3**.

The reaction of ferrocenyl ethynyl substituted triphenylamine with TCNE in a CA-RE reaction resulted in TCBD bridged **TPAs 4–8** in 60–72% yields.[32] The photophysical properties of the di-ferrocenyl TCBD bridged triphenylamine derivatives with various substituents at the phenyl ring were investigated for systems substituted with aldehyde **TPA-4**, malononitrile **TPA-5**, 1,3-indandione **TPA-6**, indanone **TPA-7** and 2-tetralonylmethylene **TPA-8** substituents (Figure 1). Two ferrocenyl-TCBD substituted phenyl groups were kept unchanged, and the acceptor at the third phenyl substituent varied. The di-TCBD bridged TPA derivatives **TPAs 4–8** exhibited two types of bands, the one at lower wavelength region at 469–502 nm corresponding to the $\pi \rightarrow \pi^*$ transition and the other one in the longer wavelength region at 630–700 nm region being related to ICT. The triphenylamine derivative with 2-tetralonylmethylene as the end capping substituent at the phenyl ring (**TPA-8**) exhibited a red shifted

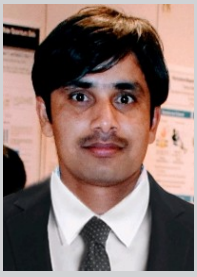

Dr. Yuvraj Patil received his PhD from Indian Institute of Technology (IIT) Indore, India, in November 2018 under the supervision of Prof. Rajneesh Misra. He received his BSc degree from SBDM, Atpadi and MSc degree from Shivaji University Kolhapur, Maharashtra (India). After completing one year as postdoc at IIT Indore, he moved to National Institute for Materials Science (NIMS), Tsukuba (Japan), in Oct. 2019 for another postdoc with Dr. Takashi Nakanishi. Currently he is working as a post-doctoral Researcher at Rennes Institute of Chemical Sciences (ISCR), University of Rennes 1 (France) with Dr. Ludovic on the development of chiro-optical materials for opto-electronics.

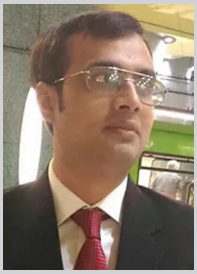

Prof. Rajneesh Misra is currently a Professor at the Department of Chemistry, Indian Institute of Technology, Indore (IIT-Indore). He obtained his Master degree from the University of Gorakhpur, India, in 2001. He moved to the Indian Institute of Technology, Kanpur, for his PhD (2007) in Chemical Sciences. After two successive postdoctoral stays at the Georgia Institute of Technology, Atlanta, USA, from 2007 to 2008 and at Kyoto University, Japan, from 2008 to 2009, he joined IIT-Indore, India, in 2009 as an Assistant Professor. His research interests lie in the areas of organic photonics and organic electronics.

Prof. Holger Butenschön obtained his doctoral degree at the University of Hamburg with Armin de Meijere in 1983. After a postdoctoral year with K. Peter C. Vollhardt at the University of California at Berkeley he performed independent research at the Max-Planck-Institute for Coal Research in Mülheim an der Ruhr, Germany. After his habilitation in organic chemistry at the University of Hamburg in 1991 he was a Heisenberg fellow (DFG) at the University of Wuppertal. Since 1993 he has been a professor of organic chemistry at Leibniz University Hannover and was a visiting professor at Kyushu University in 1999 as well as at the University of California at Berkeley in 2008. His research interests include preparative organic and organometallic chemistry of π-complexes. In 2022 he was awarded the honorary citizenship of his university.

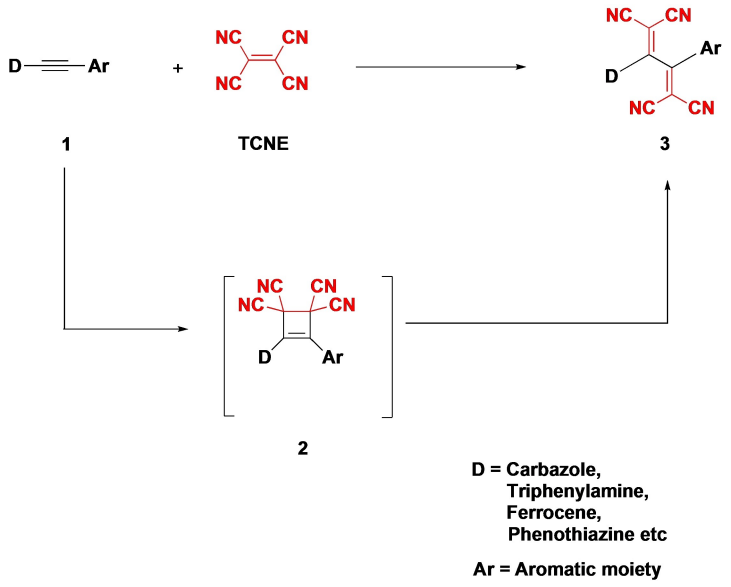

Scheme 1. CA-RE reaction sequence of TCNE to donor functionalized alkyne **1**.

absorption (502 nm) followed by the triphenylamine derivative with the indanone derived end capping substituent (**TPA-7**, 499 nm) compared to derivatives with malononitrile and aldehyde end capping substituents (**TPA-5**, 469 nm and **TPA-4**, 485 nm).

The triphenylamine derivative with indan-1,3-dione as the end capping substituent at the phenyl ring (**TPA-6**) shows a comparatively low oxidation potential of 0.39 V, whereas the triphenylamine derivative with the malononitrile end capping substituent (**TPA-5**) shows a low reduction potential of −0.94 V compared to other derivatives [(**TPA**s **4**–**8**), Table 1]. The presence of TCBD moieties and electron withdrawing end capping substituents in the molecular structure stabilizes the HOMO and LUMO energy levels. As we go from aldehyde (**TPA-4**) to 2-tetralonylmethylene (**TPA-8**), the LUMO is more stabilized compared to the stabilization of the HOMO resulting in a low HOMO-LUMO energy gap.

The optical and electrochemical investigation of **TPA**s **4**–**8** indicated a donor-acceptor interaction. The incorporation of TCBD units resulted in reduced HOMO-LUMO energy gaps in TCBD bridged **TPA**s **4**–**8** (Table 1). The DFT investigation suggested that the incorporation of the TCBD unit disturbs the coplanarity of the TCBD unit and the substituted cyclopentadienyl (Cp) ligand of the ferrocenyl moiety presumably due to steric hindrance in the molecule.

Table 1. Photophysical, electrochemical and calculated electronic properties of **TPA**s **1**–**8.**

TPA	λ_{abs} (nm) [$\varepsilon/10^4$ ($M^{-1}cm^{-1}$)]	E^2 Oxid (V)	E^1 Oxid (V)	E^1 Red (V)	E^2 Red (V)	E_g (eV)
TPA-1	510 [3.1]	–	1.20	−0.50	−1.12	2.32
TPA-2	507 [4.5]	–	1.33	−0.55	−1.14	2.42
TPA-3	494 [8.2]	–	1.35	−0.56	−1.18	2.79
TPA-4	485 [5.7]	1.11	0.41	−0.97	−1.43	2.76
TPA-5	469 [1.1]	0.99	0.42	−0.94	−1.39	2.74
TPA-6	488 [1.6]	0.98	0.39	−0.97	−1.41	2.73
TPA-7	499 [4.9]	0.93	0.43	−0.97	−1.37	2.67
TPA-8	502 [0.8]	0.89	0.44	−0.97	−1.39	2.61

E_g = HOMO-LUMO gap as calculated by DFT at B3LYP/6-31G** level for C, H and N; and at Lanl2DZ level for Fe; Potentials (V) measured versus Saturated Calomel Electrode (SCE) and referenced against FcH/FcH^+, Cyclic voltamograms (CVs) were recorded on electrochemical analyzer using Glassy carbon as working electrode, Pt wire as the counter electrode. The scan rate was 100 mVs^{-1} for CV. A solution of tetrabutylammonium hexafluorophosphate ($TBAPF_6$) in dichloromethane (0.1 M) was employed as the supporting electrolyte.

1.2. Pyrazabole Based TCBD Derivatives

Pyrazabole is an organoboron derivative, formed by of two pyrazole rings connected by two BBu_2 bridges between the respective nitrogen atoms. Pyrazabole is a weak electron acceptor and synthesized by the condensation of tributylborane and pyrazole.[33] The derivatives of pyrazabole possess excellent stability and exhibit applications in liquid crystalline materials, multiphoton absorption, mechanochromism and luminescent polymers.[34] Pyrazabole derivatives show absorption in the UV region, which limits its applicability in photovoltaics. In order to improve their electronic absorption properties, TCBD units

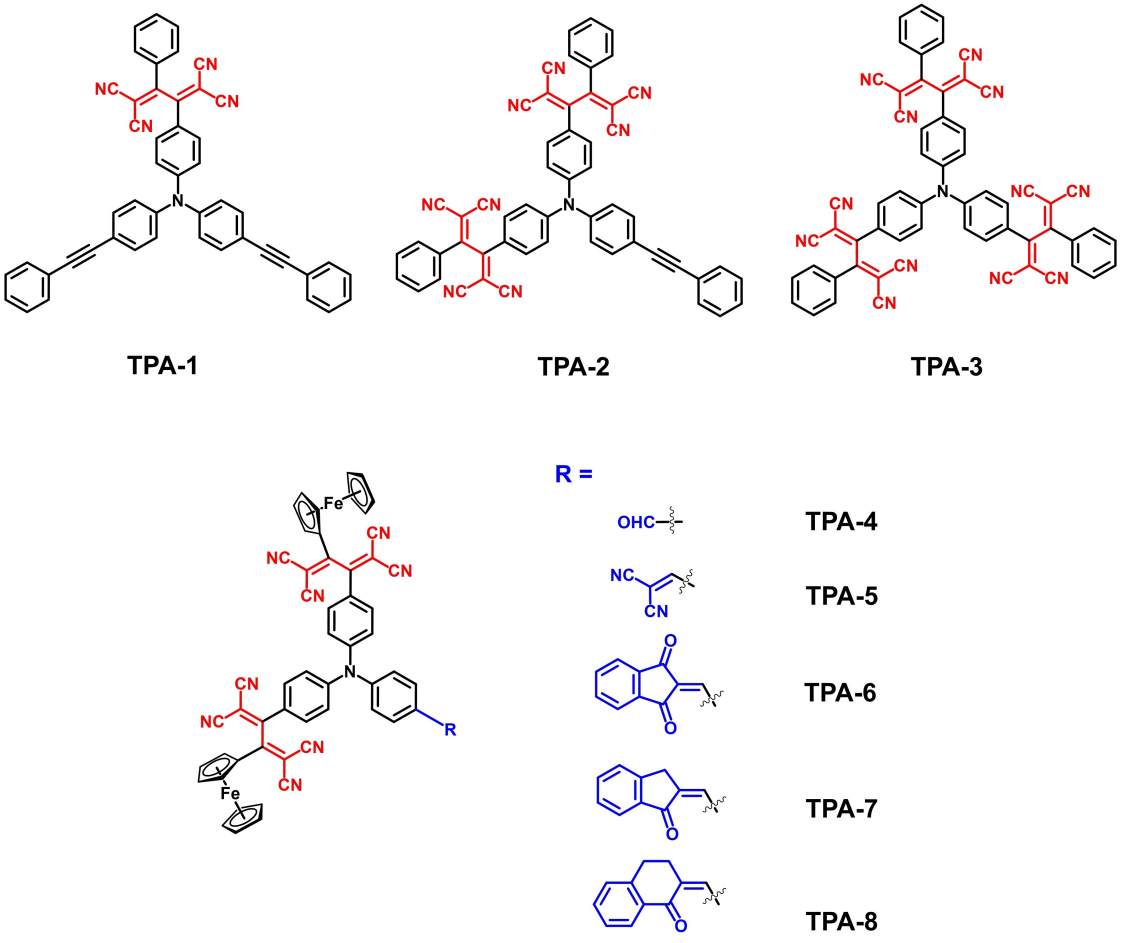

Figure 1. Chemical structures of triphenylamine based TCBD derivatives **TPAs 1–8**.

have been incorporated in ethynyl bridged donor functionalized pyrazaboles.[35]

The TCBD incorporated pyrazaboles **Fc–Pz** (85%) and **TPA–Pz** (82%) were synthesized by the CA-RE reaction sequence of ethynyl bridged pyrazabole dimers with two equivalents of TCNE (Figure 3). The di-TCBD bridged **Fc–Pz** and **TPA–Pz** show red shifted broad charge transfer bands with low HOMO-LUMO gaps compared to their ethynyl bridged dimers. The incorporation of TCBD units in the triphenylamine based pyrazabole dimer **TPA–Pz** shifts the absorption maximum from the UV region (342 nm) to the visible region (489 nm) with a substantial red shift of 147 nm (Figure 4 and Table 2), which improves its light harvesting property.

The electrochemical study revealed low reduction potential (−0.91 V) in **TPA–Pz** compared to ferrocenyl based **Fc–Pz** (−0.96 V), whereas low oxidation potential value in ferrocenyl based **Fc–Pz** (0.45 V) was observed compared to triphenylamine based **TPA–Pz** [(0.54 V), Table 2]. A strong donor-acceptor interaction between ferrocenyl/triphenylamine donor moieties and TCBD unit was observed. The shift of the absorption into the visible region, good solubility in organic solvents and high thermal stability indicate that these TCBD derivatives can be explored as a new class of promising materials for photovoltaic applications.

1.3. Truxene Based TCBD derivatives

Truxene is a planar heptacyclic aromatic system regarded as a cyclotrimer of fluorene.[36] The easy functionalization, good solubility, and thermal as well as chemical stability make truxene an important core for designing π-conjugated derivatives for applications in organic light emitting diodes (OLEDs), organic solar cells (OSCs), organic fluorescent probes and liquid crystalline materials.[37–39]

The CA-RE reaction sequence of ethynyl bridged ferrocene, triphenylamine and phenothiazine substituted truxenes with three equivalents of TCNE resulted in tri-TCBD bridged

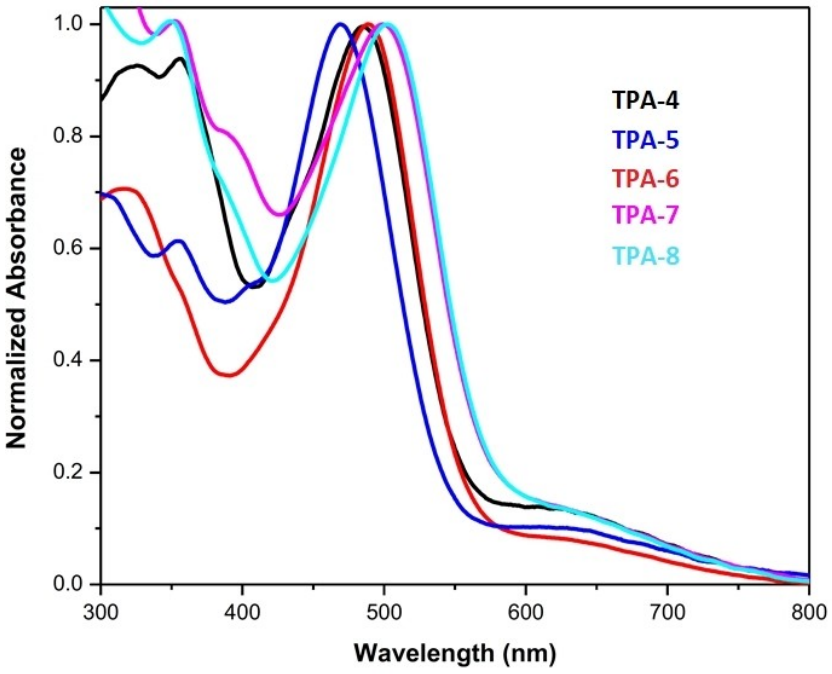

Figure 2. The normalized absorption spectra of **TPA**s **4**–**8**. Reproduced with permission from reference 32, Copyright 2014, Elsevier.

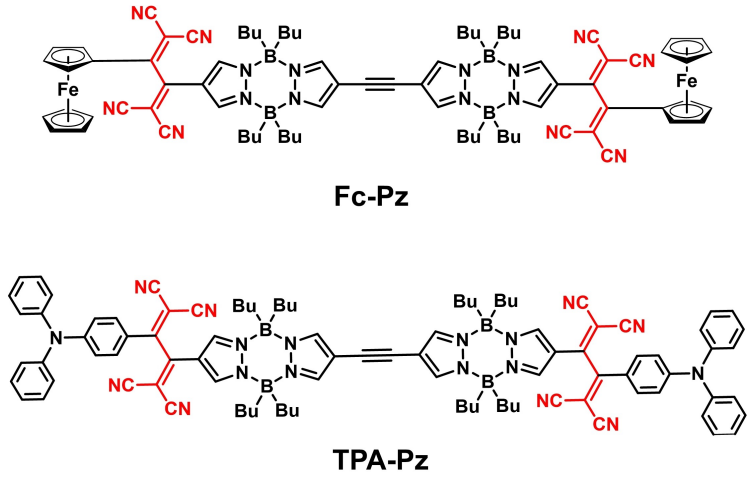

Figure 3. Chemical structures of TCBD bridged pyrazabole dimers **Fc**–**Pz** and **TPA**–**Pz**.

truxene derivatives **Fc**–**Tx** (60 %), **TPA**–**Tx** (71 %) and **Ptz**–**Tx** (65 %), respectively (Figure 5).[40] The photonic properties of tri-TCBD bridged truxenes containing ferrocenyl (**Fc**–**Tx**), triphenylamine (**TPA**–**Tx**) and phenothiazine (**Ptz**–**Tx**) end capping groups were investigated. The phenothiazine based truxene **Ptz**–**Tx** exhibits a 124 nm red shifted absorption compared to ferrocenyl truxene (**Fc**–**Tx**) and 112 nm red shifted absorption compared to triphenylamine based truxene (**TPA**–**Tx**). The ferrocenyl based truxene **Fc**–**Tx** shows a low intensity absorption band in the longer wavelength region (550 nm to 750 nm) related to a *d-d* transition of the ferrocenyl moiety. Photophysical properties of **Ptz**–**Tx** show strong ground-state interactions between the donor phenothiazine and electron-accepting TCBD units resulting in charge-transfer states which indicated good electronic communication between phenothiazine and truxene.

The cyclic voltammetry studies reveal the easier oxidation of the ferrocenyl based truxene **Fc**–**Tx** compared to the

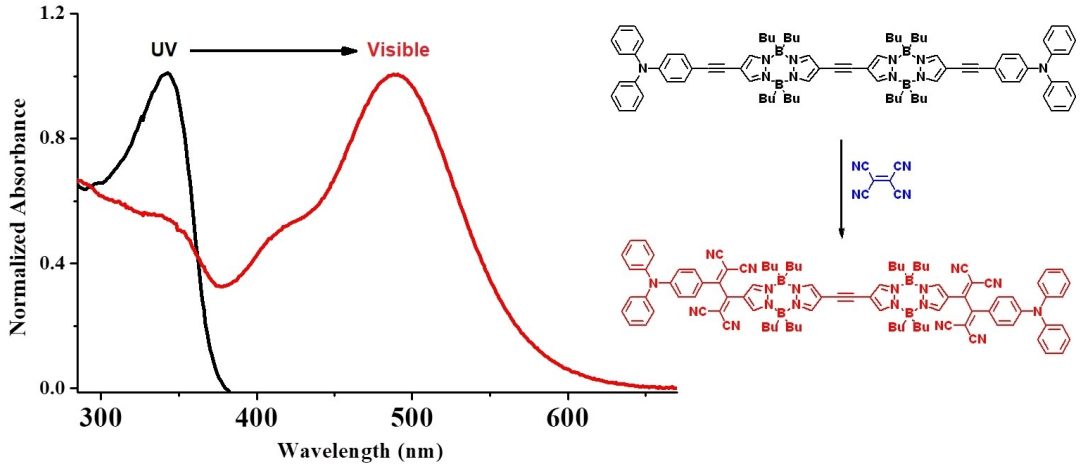

Figure 4. The normalized absorption spectra of ethyne bridged pyrazabole dimer (black line) and di-TCBD bridged pyrazabole dimer **TPA–Pz** (red line). Reproduced with permission from ref. 35a, Copyright 2017, Elsevier.

Table 2. Photophysical, thermal, electrochemical and calculated electronic properties of **Fc–Pz** and **TPA–Pz.**

Pyrazabole	λ_{abs} (nm) [$\varepsilon/10^4$ ($M^{-1}cm^{-1}$)]	T_d (°C)	E^1 Oxid (V)	E^1 Red (V)	E^2 Red (V)	E^3 Red (V)	E^4 Red (V)	E_g (eV)
Fc–Pz	345 [2.4]	291	0.45	−0.96	−1.31	−1.42	−2.01	2.94
TPA–Pz	489 [2.3]	216	0.54	−0.91	−1.22	−1.43	−2.00	1.91

E_g = HOMO-LUMO gap calculated by DFT at B3LYP/6-31G** level for C, H and N; and at Lanl2DZ level for Fe; T_d = thermal decomposition temperature (TGA).
Potentials (V) measured *versus* Ag/Ag+ electrode and referenced against FcH/FcH^+, Cyclic voltammograms and differential pulse voltammograms were recorded in dichloromethane solvent using glassy carbon as working electrode, Pt wire as the counter electrode. The scan rate was 100 mVs^{-1}. A solution of tetrabutylammonium hexafluorophosphate ($TBAPF_6$) in dichloromethane (0.1 M) was used as supporting electrolyte.

triphenylamine based truxene analogue **TPA–Tx** (Table 3 and Figure 6). The presence of metal (iron) in **Fc–Tx** exhibit easy oxidation compared to triphenylamine based **TPA–Tx**. On the other hand, the reduction of the triphenylamine based

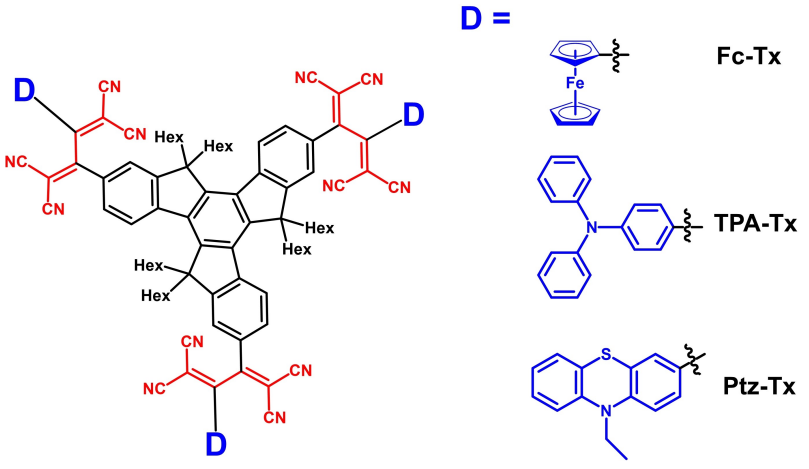

Figure 5. Donor functionalized three TCBD bridged truxene derivatives.

Table 3. Photophysical, electrochemical and calculated electronic properties of **Fc–Tx**, **TPA–Tx and Ptz–Tx.**

Truxene	λ_{abs} (nm) [$\varepsilon/10^5$ ($M^{-1}cm^{-1}$)]	E^1 Ox (V)	E^1 Red (V)	E^2 Red (V)
Fc–Tx	618, 421	0.42	−1.81	−1.92
TPA–Tx	433 [1.5]	1.30	−1.49	–
Ptz–Tx	545	0.70	−0.80	1.18

Potentials (V) measured *versus* Saturated Calomel Electrode (SCE) and referenced against FcH/FcH^+, Cyclic voltamograms (CVs) were recorded at room temperature on a CHI620D electrochemical analyser using glassy carbon as the working electrode, Pt wire as the counter electrode. The scan rate was 100 $mV\,s^{-1}$. A solution of tetrabutylammonium hexafluorophosphate ($TBAPF_6$) in dichloromethane (0.1 M) was employed as the supporting electrolyte.

truxene analogue **TPA–Tx** is easier than that of its ferrocenyl based truxene analogue **Fc–Tx**, which is consistent with the trend observed in respective pyrazabole derivatives.

1.4. Diketopyrrolopyrrole Based TCBD Derivatives

Diketopyrrolopyrrole (DPP) is a widely used electron acceptor in the design of D–A substituted extended π systems for applications in organic electronics.[41–43] The strong intramolecular hydrogen bonding and π–π interaction make DPP insoluble in organic solvents; the incorporation of alkyl chains at the nitrogen atoms of the lactam rings significantly improves its solubility. In order to increase the electron accepting ability of DPP, various electron withdrawing groups have been attached to DPP.[44]

The investigation of the effects of the substitution of various donor/acceptor substituents on the photonic, thermal and electrochemical properties of the compounds showed that the substitution of the donors and acceptors at C-3 and C-6 of the DPP can significantly perturb the photonic properties of DPP based molecular systems. The TCBD bridged symmetrical and unsymmetrical **DPPs 1–13** were synthesized by the CA-RE reaction sequence of ethynyl bridged donor functionalized DPP with TCNE (Figure 7, Yields: **DPP 1** = 91%, **DPP 2** = 85%, **DPP 3** = 70%, **DPP 4** = 91%, **DPP 5** = 65% **DPP 6** = 68% **DPP 7** = 72% **DPP 8** = 72% **DPP 9** = 70% **DPP 10** = 95% **DPP 11** = 88% **DPP 12** = 54% **DPP 13** = 67%).[43–44]

A wide variety of end capping donors including triphenylamine methoxy-substituted 4-(*N,N*-diphenylamino)phenyl, *N*-phenyl carbazole, ferrocenyl and *N,N*dimethylaminophenyl were used to tune the optoelectronic properties of DPP. The TCBD bridged phenyl DPP with *N,N*-dimethylaniline **DPP 13** showed lower absorption maxima (535 nm) and higher first reduction potentials (−1.28 V) compared to thienyl DPP derivatives with other donor substituents [**DPP 1–12**, Table 4]. The di-TCBD bridged thienyl DPPs exhibited lower first reduction potentials due to the presence of two electron withdrawing TCBD moieties. The effect of the number of TCBD incorporations was investigated and showed that, as the number of TCBD units in the molecule increases, red shift in the absorption was observed indicating lowering of the HOMO-LUMO energy gap. The effect of the first TCBD incorporation was more pronounced as compared to the second TCBD incorporation. The analysis of Figure 8 and Table 4 shows that, as the number of donor and acceptor substitutions at C-3 and C-6 of the DPP increases, significant red shift in the absorption spectrum was observed. Thermogravimetric analysis (TGA) showed the ferrocenyl substituted DPPs are thermally more stable than other donor functional-

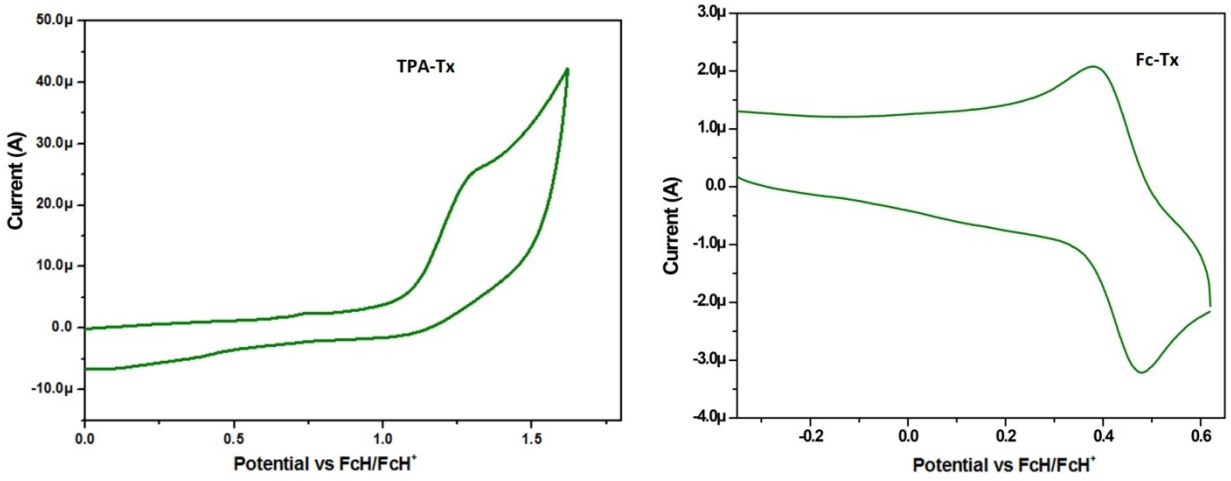

Figure 6. Cyclic voltammogram of TCBD bridged **TPA–Tx** and **Fc–Tx** (1.0×10^{-4} M). Figure reproduced from Reference 40b.

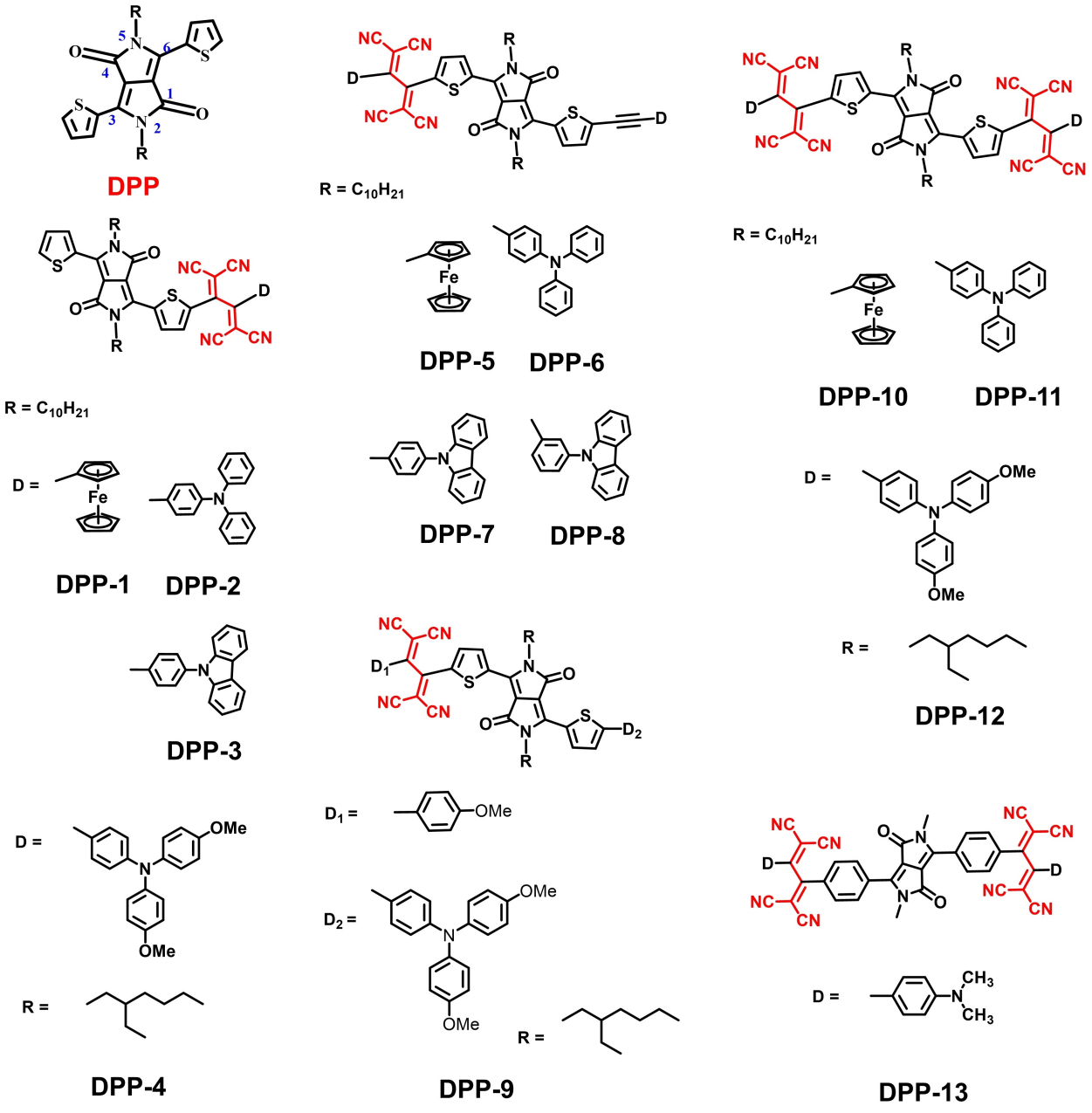

Figure 7. Chemical structures of mono/di-TCBD bridged **DPPs 1–13**.

ized DPPs. The ferrocenyl based di-TCBD bridged **DPP 10** showed a small HOMO-LUMO gap (0.71 eV) compared to its other mono-TCBD bridged DPP derivatives **1** (0.98 eV) and **5** (0.88 eV). On the other hand, in case of triphenylamine substituted TCBD bridged DPPs, the mono-TCBD bridged DPPs with additional donor units (**6** and **9**) show lower HOMO-LUMO gaps compared to other mono- and di-TCBD bridged DPPs due to strong electronic communication between triphenylamine and acceptors.

Significant color changes were observed in day light after the incorporation of TCBD in ethyne linked DPPs (e.g. *N*-phenylcarbazole substituted DPP, Figure 8). The TCBD bridged DPPs show systematic red shift of the absorption spectra with decrease in HOMO-LUMO energy gap compared to their ethynyl bridged precursors. The diketopyrrolopyrrole derivatives with D–A substitution exhibit strong absorptions in the visible to NIR region and can be regarded as potential candidates for organic photovoltaics. In addition, the DPP

Table 4. Photophysical, thermal, electrochemical and calculated electronic properties of **DPP**s **1**–**13**.

DPP	λ_{abs} (nm) [$\varepsilon/10^4$ ($M^{-1}cm^{-1}$)]	T_d (°C)	E^4 Ox (V)	E^3 Ox (V)	E^2 Ox (V)	E^1 Ox (V)	E^1 Red (V)	E^2 Red (V)	E^3 Red (V)	E^4 Red (V)	E_g (eV)
DPP 1	681 [4.8]	379	–	1.07	0.75	0.56	−0.74	−1.01	−1.55	−1.85	0.98
DPP 2	683 [1.7]	357	–	1.42	0.89	0.73	−0.70	−0.93	−1.31	–	1.43
DPP 3	695 [4.8]	266	–	–	1.18	0.26	−0.73	−1.01	−1.46	–	0.99
DPP 4	691 [3.7]	-	–	1.02	0.68	0.54	−0.82	−1.02	−1.88	–	1.36
DPP 5	725 [4.0]	373	0.98	0.70	0.46	0.13	−0.79	−1.00	−1.50	−1.78	0.88
DPP 6	728 [3.1]	366	1.12	0.88	0.74	0.56	−0.79	−1.00	−1.55	−2.18	1.35
DPP 7	726 [4.8]	329	–	–	0.77	0.51	−0.72	−1.00	−1.46	–	1.23
DPP 8	723 [6.3]	367	–	1.38	0.98	0.73	−0.56	−0.85	−1.38	–	1.29
DPP 9	796 [6.1]	-	–	1.02	0.65	0.25	−0.76	−1.01	−1.85	–	1.01
DPP 10	732 [4.9]	410	–	–	0.96	0.57	−0.55	−0.64	−1.20	−1.90	0.71
DPP 11	738 [1.9]	338	–	–	1.41	0.90	−0.59	−1.04	−1.26	1.90	1.49
DPP 12	749 [4.8]	–	–	1.02	0.89	0.55	−0.63	−0.71	−1.14	−2.00	1.17
DPP 13	535 [2.4]	–	–	–	–	–	−1.28	−1.60	−2.38	–	–

E_g = HOMO-LUMO gap as calculated from electrochemical data (CV); T_d = thermal decomposition temperature (TGA); Potentials (V) measured *versus* Ag/Ag+ electrode and referenced against FcH/FcH^+, Cyclic voltammograms and differential pulse voltammograms were recorded in dichloromethane solvent using glassy carbon as working electrode, Pt wire as the counter electrode. The scan rate was 100 $mV\,s^{-1}$. A solution of tetrabutylammonium hexafluorophosphate ($TBAPF_6$) in dichloromethane (0.1 M) was used as supporting electrolyte.
*For electrochemical investigation of **DPP 4**, **DPP 9**, **DPP 12**, Pt electrode was used as working electrode.

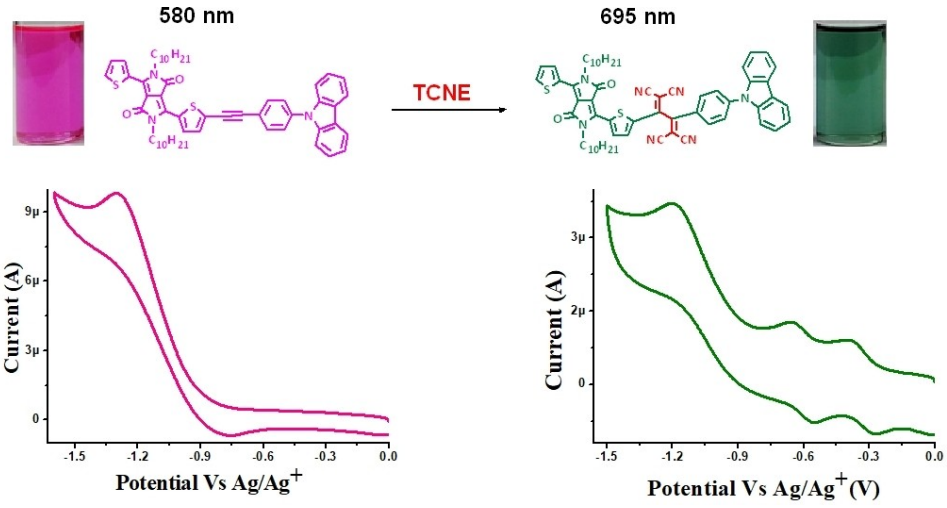

Figure 8. Effect of incorporation of TCBD to ethynyl bridged *N*-phenylcarbazole based DPP. Reproduced from ref. 44c with permission from Wiley-VCH Verlag GmbH & Co. KGaA, Copyright 2016.

derivatives exhibit good thermal stability and low HOMO-LUMO gaps required for the applicability of materials as donor/acceptor components in organic photovoltaics.[45] The electron accepting ability of DPP has been improved by incorporation of TCBD, and for the first time triphenylamine functionalized TCBD linked materials (**DPP**s **2** and **11**) have been used as non-fullerene acceptors in organic solar cells[43] (OSCs) with respectable power conversion efficiency, which is further discussed in the application section.

Recently phenothiazine based TCBD bridged donor-acceptor **DPP**s **14**–**16** were synthesized (Figure 9) and demonstrated the intervalence charge transfer (IVCT) process in **16**.[46] IVCT is a type of CT band commonly observed in mixed valence compounds or in the systems where two metal sites differing only in oxidation state. The IVCT compound **16** consist of a multi-redox centre in a single molecular structure having TCBD incorporated to the phenothiazine-bis(thienyl)DPP molecular system.

The DPPs **14**–**16** exhibit absorption maxima at 694, 736 and 753 nm, respectively. The compounds containing the highly electron deficient TCBD entity (**14**–**16**) do not show a significant emission which may be due to self-absorption or/

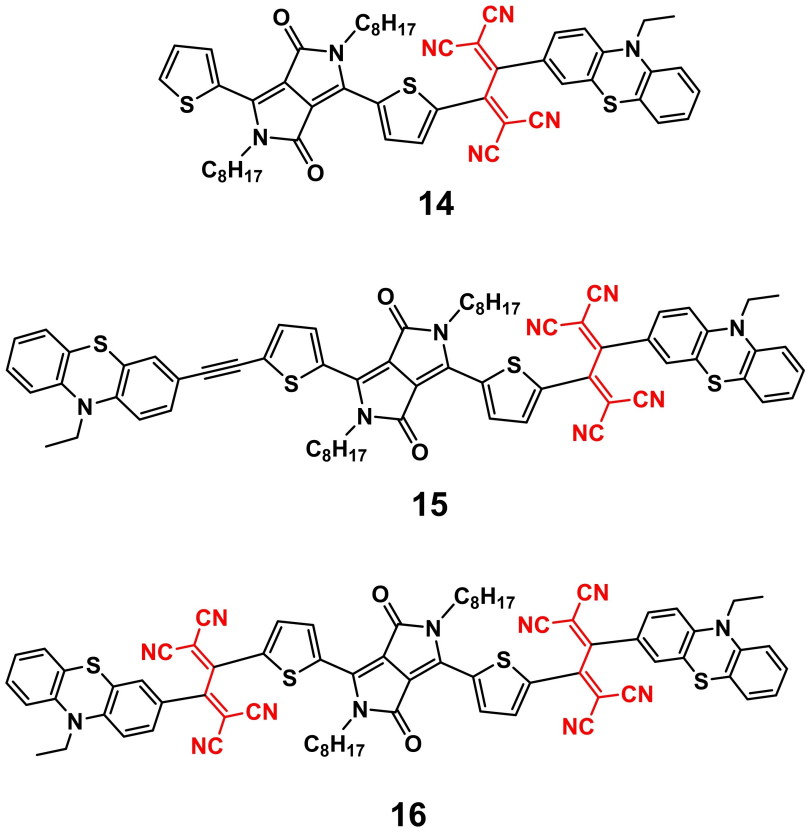

Figure 9. Chemical structures of mono/di-TCBD bridged phenothiazine functionalized DPPs.

and photoinduced charge transfer from donor to acceptor moieties in push-pull systems. The first evidence for the occurrence of electron exchange event in **16** was the splitting of TCBD reduction wave as demonstrated by the electrochemical studies. The electron exchange process was further confirmed by spectro-electrochemical studies which revealed the anticipated intra-valence charge transfer band in the NIR range (Figure 10). The origin of the IVCT transition in the NIR region was caused by the one-electron reduction of the

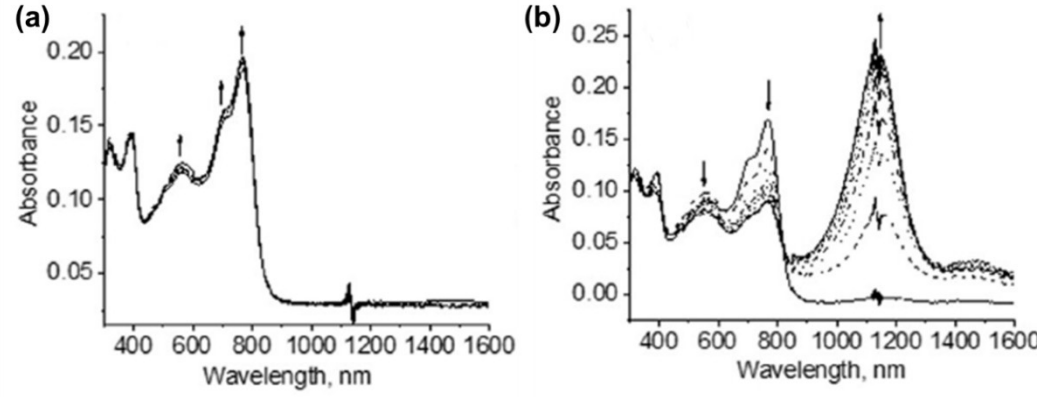

Figure 10. Spectral changes observed during first oxidation and first reduction of compounds **16** (a and b) recorded in DCB containing 0.2 M TBA(ClO_4). Reproduced with permission from ref. 46, Copyright 2017, Wiley.

TCBD unit that encouraged the electron exchange process between the two TCBD entities.

1.5. Isoindigo Based TCBD Derivatives

Isoindigo is a classical electron-deficient unit and can be synthesized at low cost for various optoelectronic applications.[47] It has been used for pharmaceutical applications as an antiproliferative agent.[48] Isoindigo possesses a broad planar structure, absorption in the visible region, and high photochemical stability.[49] It has been applied in the design of donor-acceptor (D–A) based small molecules and polymers.[50]

Recently we reported the triphenylamine functionalized mono- and di-TCBD bridged isoindigo derivatives (**Isoindigo 1** (90 %) and **2** (93 %), Figure 11), which were synthesized by CA-RE reaction of ethynyl linked triphenylamine functionalized isoindigo with one and two equivalents of TCNE.[51]

The electronic absorption spectrum of mono-TCBD bridged **Isoindigo 1** shows two distinct absorption bands at ca. 457 nm due to π–π^* transition and at 594 nm related to the intramolecular charge transfer (ICT) transition. The di-TCBD bridged **Isoindigo 2** possesses two absorption bands at ca. 475 nm and at 554–710 nm due to the π–π^* and the ICT transition, respectively. **Isoindigo 1** (mono-TCBD derivative) shows a red-shift in the absorption spectra compared to **Isoindigo 2** (di-TCBD derivative), due to more twisted backbones in the molecular structure of **Isoindigo 2** after incorporation of the additional TCBD unit.

The triphenylamine functionalized mono- and di-TCBD bridged isoindigo derivatives (**Isoindigo 1** and **2**) exhibit three reduction waves. The first two out of three reduction waves at −0.70 V, −0.97 V in **Isoindigo 1** and at −0.57 V, −1.16 V in **Isoindigo 2** are due to TCBD unit. The third reduction wave in **Isoindigo 1** and **2** at around −1.25 V and −1.27 V is related to the isoindigo unit (Table 5). The lower reduction values for TCBD unit(s) compared to the isoindigo unit indicate the strong acceptor nature of TCBD. **Isoindigo 1** shows two oxidation waves at 0.57 V and at 0.85 V due to the substitution of the triphenylamine moiety, whereas the di-TCBD bridged TCBD **Isoindigo 2** exhibits one oxidation wave around 0.85 V. The results of photophysical and DFT studies showed that the mono-TCBD bridged ethynyl functionalized isoindigo derivatives exhibited red shifted electronic absorption with low HOMO-LUMO gap values.

Table 5. Photophysical, electrochemical and computational properties of **Isoindigo 1** and **2**.

Isoindigo	λ_{abs} (nm) [$\varepsilon/10^4$ ($M^{-1}cm^{-1}$)]	E^1 Ox (V)	E^2 Ox (V)	E^1 Red (V)	E^2 Red (V)	E^3 Red (V)	E_g (eV)
1	594 [2.4]	0.57	0.85	−0.70	−0.97	−1.25	1.81
2	475 [5.6]	0.85	–	−0.57	−1.16	−1.27	1.95

E_g = HOMO-LUMO gap as calculated by DFT at B3LYP/6-31G** level for C, H and N;
Potentials (V) measured versus Saturated Calomel Electrode (SCE) and referenced against FcH/FcH^+, Cyclic voltammograms and differential pulse voltammograms were recorded on a CHI620D electrochemical analyzer in dichloromethane solvent and potentiostat using glassy carbon as working electrode, Pt wire as the counter electrode. The scan rate was 100 mVs^{-1} for cyclic voltammetry. A solution of tetrabutylammonium hexafluorophosphate ($TBAPF_6$) in dichloromethane (0.1 M) was used as supporting electrolyte.

1.6. Phenothiazine Based TCBD Derivatives

Phenothiazine is an electron-rich tricyclic heterocycle containing sulfur and nitrogen atoms.[52–53] The derivatives of phenothiazine exhibit good thermal stability and have been explored for various optoelectronic applications.[54–55] The phenothiazines **Phen 1**–**7** were designed by varying the number and the nature of the end capping donor and acceptor TCBD units in the molecule. The ferrocenyl and triphenylamine based phenothiazines **Phen 1**–**7** were prepared by CA-RE reaction of ethynyl linked donor functionalized phenothiazines with TCNE in 80–90 % yield (Figure 12).[56]

The mono-TCBD bridged ferrocenyl phenothiazine **Phen 3** shows the absorption maximum at 531 nm, further incorporation of a ferrocenylethynyl group at C-7 red shifted the absorption maxima to 547 nm in **Phen 1**. The incorpo-

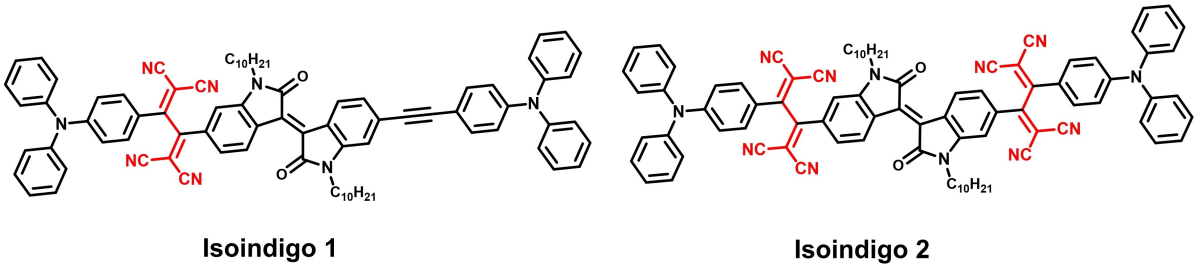

Figure 11. Chemical structures of mono/di-TCBD bridged **Isoindigo** derivatives **1** and **2**.

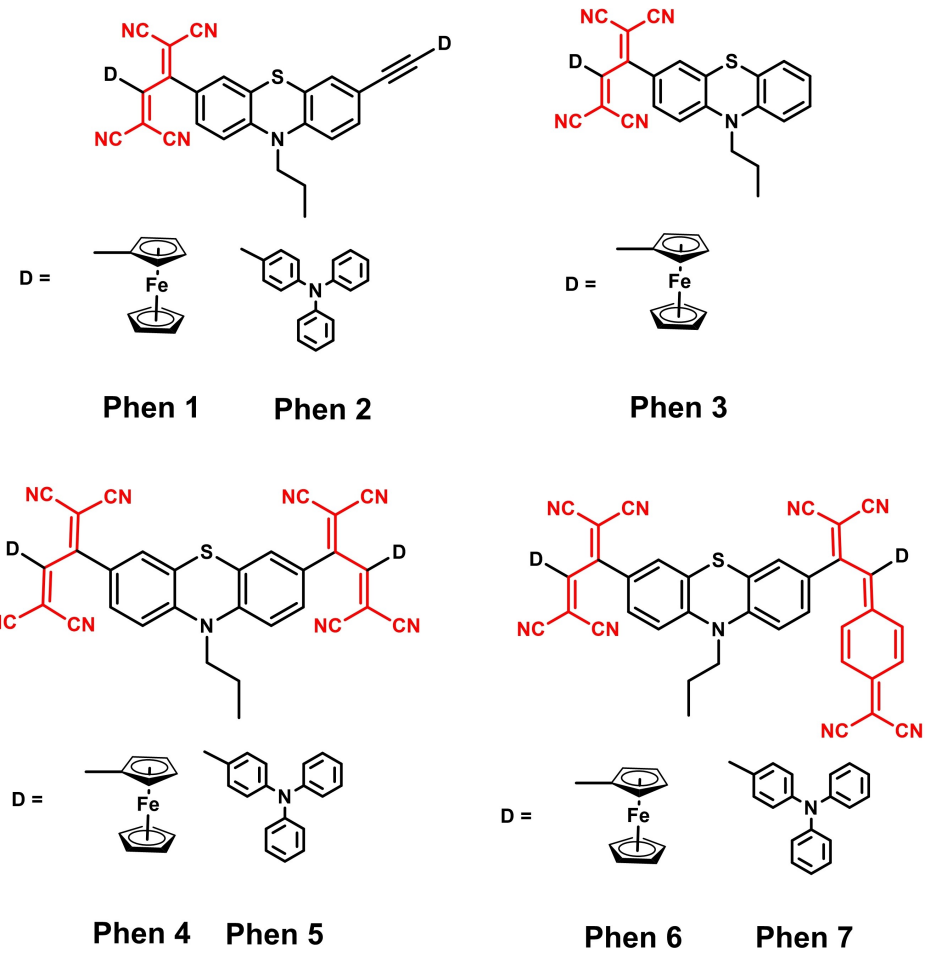

Figure 12. Chemical structures of mono/di TCBD substituted phenothiazines **Phen 1**–7.

ration of a second TCBD unit in **Phen 1** showed blue shift of absorption by 10 nm in **Phen 4** (537 nm). The incorporation of stronger acceptor TCNQ to **Phen 1** resulted in blue shift of absorption by 23 nm in **Phen 6**, which exhibits its absorption maximum at 521 nm. The mono-TCBD bridged triphenylamine based phenothiazine **Phen 2** shows absorption at 498 nm, and incorporation of a second TCBD caused a blue shift of 6 nm **(Phen 5)**. On the other hand, incorporation of the stronger acceptor TCNQ unit to **Phen 2** red shifts the absorption by 150 nm [**Phen 7**, Table 6].

The incorporation of TCNQ in **Phen 1** and **Phen 2** results in **Phen 6** and **Phen 7**. The ferrocenyl functionalized phenothiazine derivative **Phen 6** shows blue shifted electronic absorption spectra compared to **Phen 1**, whereas triphenylamine functionalized **Phen 7** shows a red shift of the absorption compared to **Phen 2**. The trend in HOMO-LUMO gap calculated from DFT calculations is consistent with the experimental absorption wavelengths for triphenylamine substituted TCBD/DCNQ bridged phenothiazines.

In case of triphenylamine based **Phen 2** the blue shift in absorption was observed after incorporation of TCBD (in **Phen 5**) whereas TCNQ incorporation leads to red shift in absorption spectra (in **Phen 7**). On the other hand, in case of ferrocenyl based **Phen 1** the incorporation of TCBD and TCNQ units led to blue shift in absorption (in **Phen 4** and **6**).

The effect of the number of TCBD units and the nature of the end capping donor on the photonic and electronic properties were investigated, revealing that the TCBD derivatives with triphenylamine donor (**Phen 2**, **5** and **7**) showed low HOMO-LUMO gap values compared to the TCBD derivatives with a ferrocenyl donor (**Phen 1**, **3**, **4** and **6**). The electrochemical study showed lower reduction potentials in triphenylamine based phenothiazines (**Phen 2**, **5** and **7**) compared to ferrocenyl phenothiazines (**Phen 1**, **3**, **4** and **6**). On the other hand, lower oxidation potentials were observed in ferrocenyl phenothiazines (**Phen 1**, **3**, **4** and **6**) compared to triphenylamine based phenothiazines [(**Phen 2**, **5** and **7**)

Table 6. Photophysical, electrochemical and calculated electronic properties of phenothiazines **Phen 1**–**Phen 7**.

Phenothi-azine	λ_{abs} (nm) [$\varepsilon/10^4$ ($M^{-1}cm^{-1}$)]	E^3 Ox (V)	E^2 Ox (V)	E^1 Ox (V)	E^1 Red (V)	E^2 Red (V)	E^3 Red (V)	E^4 Red (V)	E_g^d (eV)
Phen 1	547 [6.8]	0.41	0.28	−0.07	−1.16	−1.46	–	–	2.49
Phen 2	498 [1.7]	0.68	0.49	0.36	−0.98	−1.28	–	–	2.07
Phen 3	531 [6.5]	–	–	0.31	−1.15	−1.44	–	–	2.64
Phen 4	537 [7.0]	–	0.28	0.55	−1.12	−1.47	–	–	2.63
Phen 5	492 [4.0]	–	–	0.70	−0.92	−1.27	–	–	2.37
Phen 6	524 [7.7]	0.45	0.27	0.16	−0.94	−1.23	−1.51	–	2.28/2.11
Phen 7	650 [3.6]	–	0.57	0.39	−0.77	−0.88	−1.04	−1.33	1.77

E_g = HOMO-LUMO gap as calculated by DFT at B3LYP/6-31G** level for C, H and N; and at Lanl2DZ level for Fe; Potentials (V) measured versus Saturated Calomel Electrode (SCE) and referenced against FcH/FcH^+. Cyclic voltammograms and differential pulse voltammograms were recorded on potentiostat using glassy carbon as working electrode, Pt wire as the counter electrode at room temperature. The scan rate was 100 $mV\,s^{-1}$. A solution of tetrabutylammonium hexafluorophosphate ($TBAPF_6$) in dichloromethane (0.1 M) was used as supporting electrolyte.

Table 6]. The donor-acceptor interaction was observed between donor moieties (ferrocenyl and triphenylamine) and the acceptor TCBD unit.

1.7. BODIPY Based TCBD Derivatives

BODIPY dyes have attracted the attention of the scientific community due to their strong accepting nature, good solubility in organic solvents, strong electronic absorption with high absorption coefficients and tunable redox potentials.[57] The derivatives of BODIPY have been used for the applications in cell imaging, logic gates and organic photovoltaics.[58–61] The photonic and electronic properties of BODIPY dyes can be tuned by substitution of different donor groups at α, β and *meso*-positions.

The mono TCBD bridged ferrocenyl derivatives of *meso*-BODIPYs **BOD**s **1–5** (Figure 13) show the same distance between the donor (ferrocenyl/triphenylamine/phenothiazine) and TCBD moieties with varying distance between BODIPY to the TCBD unit.[62–63] These **BOD**s **1–5** were synthesized by CA-RE reaction in 65–95 % yield. The TCBD and BODIPY moieties were connected directly by a single bond (in **BOD 1**), by a phenylethynyl linkage (in **BOD 2**), by a vinylene linkage (in **BOD 3**), or phenyl linkages (in **BODs 4** and **5**). The BODIPY **BOD 1**, in which TCBD is directly linked with the BODIPY core, exhibits a red shifted absorption compared to the BODIPY derivatives in which TCBD is attached to BODIPY *via* a phenyl acetylene linkage (in **BOD 2)** or by a vinyl linkage (in **BOD 3**). The cyclic voltammetry study reveals the lower oxidation potential of mono-TCBD bridged ferrocenyl based **BODs 1–3** compared to mono-TCBD bridged triphenylamine/phenothiazine-based **BOD 4/5** (Table 7). On the other hand, the reduction of triphenylamine/

Table 7. Photophysical, electrochemical and calculated electronic properties of **BOD**IPYs **1–5**.

BODIPY	λ_{abs} (nm) [$\varepsilon/10^4$ ($M^{-1}cm^{-1}$)]	E^3 Ox (V)	E^2 Ox (V)	E^1 Oxid (V)	E^1 Red (V)	E^2 Red (V)	E^3 Red (V)	E^4 Red (V)	E_g (eV)
BOD 1	567 [3.4]	–	1.28	0.52	−0.35	−0.71	−1.32	−1.80	2.22
BOD 2	561 [4.9]	–	1.21	0.48	−0.79	−0.88	−1.16	−1.29	2.31
BOD 3	521 [4.5]	1.34	1.10	0.40	−0.73	−1.42	−2.03	−2.23	1.84
BOD 4	–	–	1.71	1.36	−0.20	−0.56	−0.91	–	–
BOD 5	–	–	1.67	1.04	−0.10	−0.47	−0.79	–	1.97

E_g = HOMO-LUMO gap as calculated by DFT at B3LYP/6-31G** level for C, H and N; and at Lanl2DZ level for Fe; Potentials (V) measured versus Saturated Calomel Electrode (SCE) and referenced against FcH/FcH^+.
For **BODIPY**s **1—3:** Cyclic and differential pulse voltammograms were recorded on a CHI620D electrochemical analyser in dichloromethane solvent and 0.1 M TBAF6 as the supporting electrolyte at room temperature. The electrodes used were glassy carbon as a working electrode, Pt wire as a counter electrode and the saturated calomel electrode as a reference electrode.
For **BODIPY**s **4** and **5:** Differential pulse and cyclic voltammograms were recorded on an EG&G PARSTAT electrochemical analyzer using a three electrode system. A platinum button electrode was used as the working electrode. A platinum wire served as the counter electrode and an Ag/AgCl electrode was used as the reference electrode. The analysis was performed in benzonitrile at room temperature using tetrabutylammonium perchlorate, $(TBA)ClO_4$, as a supporting electrolyte.

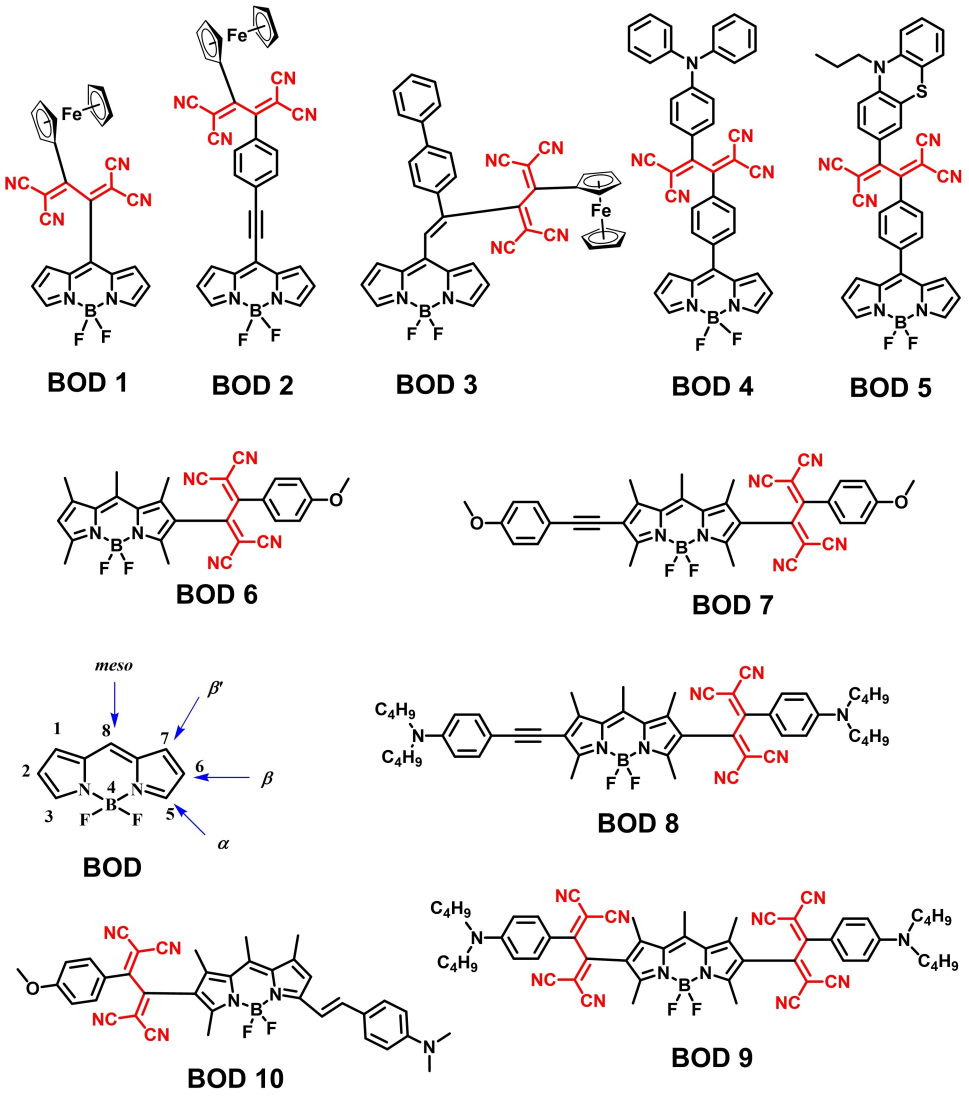

Figure 13. Chemical structures of mono-/di-TCBD bridged BODIPYs **BODs 1–10**.

phenothiazine-based **BOD 4/5** is easier than that of ferrocenyl **BODs 1–3**.

Ziessel *et al.* reported symmetrical and unsymmetrical TCBD bridged *β*-BODIPYs with various end capping donors **BOD 6–BOD 10** in different yields ranging from a low yield of 36% (**BOD 9**) to a high yield 81% (**BOD 10**) for NLO applications.[64] The **BODs 6–10** show absorption bands at 475, 543, 574, 558 and 599 nm, respectively, and exhibited molar absorption coefficients between 35000–80000 $M^{-1}\cdot cm^{-1}$. The effect of the change in the end capping donor and the number of TCBD units on the photophysical and electrochemical properties was studied. In the case of *N,N*-dimethylaniline and anisole substituted TCBD linked BODIPYs, it was observed that BODIPYs with two electron donating substituents attached to the *β*-position (**BODs 6–10**) exhibit red shifted absorptions compared to TCBD bridged BODIPY with only one donating substituent (**BOD 6**). The incorporation of a second TCBD unit to *N,N*-dimethylaminophenyl substituted **BOD 8** causes a blue shift of the absorption from 574 nm to 558 nm in **BOD 9**, which indicates poor electronic communication in di-TCBD bridged **BOD 9**. The mono-TCBD bridged anisole-based **BOD 6** exhibits an absorption maximum at 475 nm, and further substitution of ethynyl anisole at the *β*-position (**BOD 7**) causes a blue shift in the electronic absorption. On the other hand the substitution of *N,N*-dimethylaniline at the *α*-position *via* a double bond improves the conjugation which lead to red shift in the absorption spectra (599 nm).

Recently *N*-analogue of BODIPY *i. e.* Aza-BODIPY with high energy charge transfer with panchromatic absorption has been reported (Figure 14).[65] Donor-acceptor system was made by connecting triphenylamine (TPA) to TCBD, a high energy charge transfer system which then linked to Aza-BODIPY, the NIR sensitizer for the promotion of excited state charge separation. Here successful demonstration of efficient charge separation upon both high-energy charge transfer and low-energy NIR excitations indicating the importance of this donor-acceptor system for optoelectronic applications with wide optical window from UV-Vis to NIR.

1.8. Benzothiadiazole (BTD) Based TCBD Derivatives

Benzo[*c*][1,2,5]thiadiazole (BTD) is an electron-withdrawing moiety widely used for developing various small molecules and polymers as semiconductors.[66] BTD contains a diazole ring fused with a benzene ring, in which one of the carbon atoms in the diazole ring is replaced by a sulfur atom.

The TCBD bridged ferrocenyl and triphenylamine based **BTD**s **1–6** were synthesized by the CA-RE reaction sequence in 70–85 % (Figure 15).[25b,67] The ferrocenyl TCBD substituted BTD with triphenylamine as end capping donor **BTD 2**

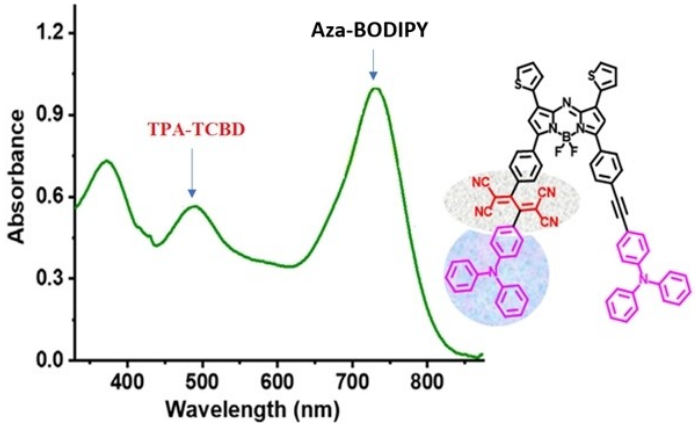

Figure 14. Chemical structure and absorption spectra of TCBD bridged Aza-BODIPY. Reproduced from ref. 65 with permission from Wiley-VCH Verlag GmbH & Co. KGaA, Copyright 2020.

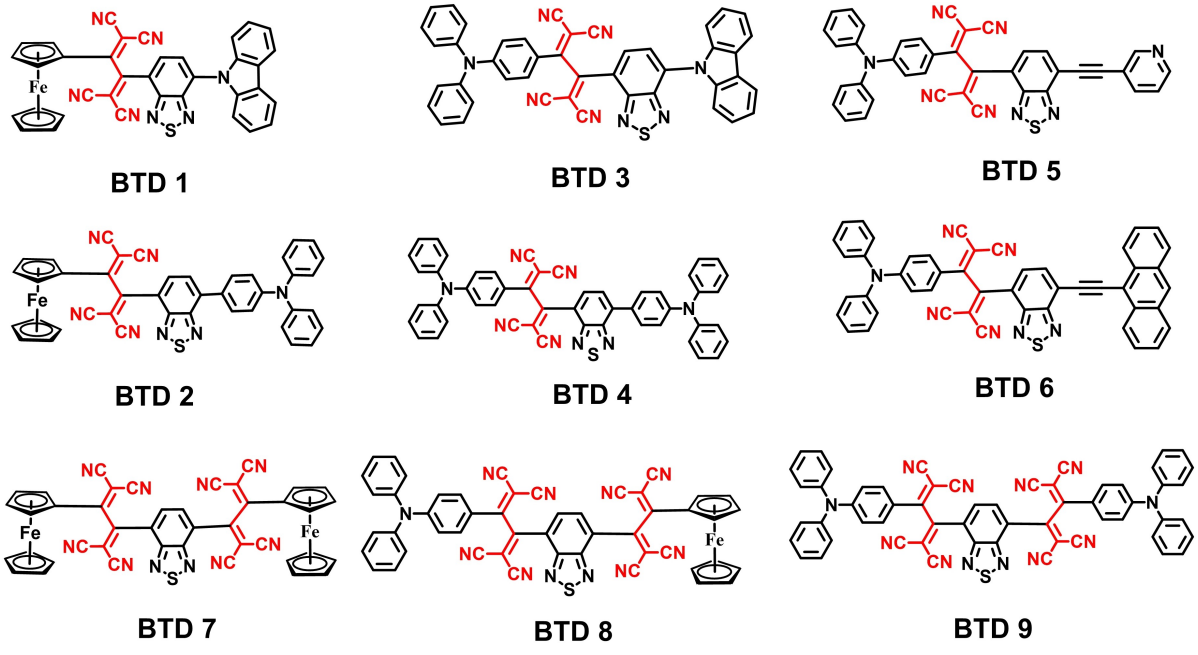

Figure 15. Chemical structures of mono-/di-TCBD bridged **BTD**s **1–9**.

showed a red shift of the absorption by 52 nm compared to ferrocenyl TCBD substituted BTD with carbazole as end capping donor **BTD 1**. The electrochemical study shows that **BTD 2** exhibited easier oxidation and harder reduction compared to **BTD 1**. The triphenylamine-TCBD substituted **BTD 4** with triphenylamine end capping donor on another side showed an absorption maximum at 560 nm. Study of the effect of the end capping donor in triphenylamine based TCBD derivatives reveals that the substitution of a triphenylamine unit with BTD by a direct bond as in **BTD 4** gives a red shifted absorption (560 nm) compared to substitution of 3-pyridylethynyl (**BTD 5**, 446 nm), 9-anthracenylethynyl (**BTD 6**, 545 nm), and *N*-phenyl carbazole (**BTD 3**, 518 nm) substitutions.

The electrochemical data (Table 8) reveal that the oxidation of triphenylamine based **BTD**s **3–6** is harder compared to ferrocenyl **BTD**s **1** and **2**. On the other hand, the reduction of ferrocenyl **BTD**s **1** and **2** is difficult compared to triphenylamine based **BTD**s **3–6**. The effect of the nature of the end capping group on the photonic and electronic properties indicates that the 3-pyridylethynyl based **BTD 5** with triphenylamine as the donor shows a low HOMO-LUMO gap value compared to the other TCBD derivatives.

The di-TCBD bridged symmetrical and unsymmetrical donor (ferrocenyl/triphenylamine) based **BTDs 7–9** were synthesized by the CA-RE reaction sequence of ethynyl bridged ferrocenyl/triphenylamine based BTD derivatives with two equivalents of TCNE with high yields (85–94 %).[68]

The unsymmetrical donor (ferrocene and triphenylamine) substituted TCBD bridged **BTD 8** showed a red shift in electronic absorption compared to di-ferrocenyl and di-triphenylamine functionalized TCBD bridged **BTD**s **7** and **9**. The electrochemical study showed that the di-TCBD bridged unsymmetrical **BTD 8** undergo two oxidations, one at 0.50 V and another one at 0.83 V due to the ferrocene and triphenylamine moieties, respectively (Table 8). On the other hand, only one oxidation wave was observed in the case of symmetrical ferrocenyl based **BTD 7** (at 0.50 V) and triphenylamine based **BTD 9** (at 0.64 V). The **BTD**s **7–9** show three reduction waves in their cyclic voltammograms, the first two reduction waves are due to the TCBD unit(s) and the third one is due to the BTD unit. The reduction of di-TCBD bridged **BTD**s **7–9** is easier compared to mono-TCBD bridged BTD derivatives (**BTD**s **1–6**). The donor-acceptor interaction was observed from the ferrocenyl/triphenylamine donor moieties to the acceptor TCBD unit. The effect of the number of TCBD units on the photonic and electronic properties causes the di-TCBD bridged BTD derivatives (**BTDs 7–9**) to show broad absorption, easier reduction and low HOMO-LUMO gap values compared to the mono-TCBD bridged BTD derivatives with ferrocenyl donor (**BTDs 1–6**).

1.9. Pyrene Based TCBD Derivatives

Pyrene is the smallest peri-fused polycyclic aromatic hydrocarbon and has been explored for optoelectronic applications.[69] It is a well-known donor and exhibits a good fluorescence quantum yield.[70] In order to evaluate the effect of TCBD on its photonic and electrochemical properties, the colored mono-TCBD linked ferrocenyl substituted pyrenes **Fc–Py 1** (80 %) and **Fc–Py 2** (85 %) were synthesized by the CA-RE reaction sequence of ethynyl bridged ferrocenyl substituted pyrenes with TCNE (Figure 16).[71]

Fc–Py 1 exhibits two strong charge transfer bands, one is due to charge transfer from the ferrocenyl substituent to TCBD at 639 nm and another one from pyrene donor to the TCBD acceptor at 474 nm (Table 9). On the other hand,

Table 8. Photophysical, electrochemical and calculated electronic properties of **BTD**s **1–9**.

BTD	λ_{abs} (nm) [$\varepsilon/10^4$ (M^{-1} cm^{-1})]	E^3 Ox (V)	E^2 Ox (V)	E^1 Ox (V)	E^1 Red (V)	E^2 Red (V)	E^3 Red (V)	E_g (eV)
BTD 1	502 [4.6]	0.42	0.22	0.02	−1.23	−1.59	−2.48	2.62
BTD 2	554 [6.1]	–	0.18	0.01	−1.25	−1.69	−2.55	2.37
BTD 3	466 [4.9], 518	–	0.78	0.57	−0.76	−1.23	−1.43	2.46
BTD 4	560 [3.4]	–	0.75	0.54	−0.83	−1.21	−1.422	2.40
BTD 5	446 [6.2]	–	–	0.88	−0.75	−1.13	–	1.69
BTD 6	545 [5.9]	–	–	0.91	−0.83	−1.19	−2.07	2.17
BTD 7	618 [4.3]	–	–	0.50	−0.52	−0.66	−1.40	2.17
BTD 8	624 [4.2]	–	0.83	0.50	−0.51	−0.67	−1.36	1.83
BTD 9	490 [6.0]	–	–	0.64	−0.55	−0.70	−1.36	2.03

Potentials (V) measured versus Saturated Calomel Electrode (SCE) and referenced against FcH/FcH^+; Glassy carbon was used as working electrode and Pt wire as the counter electrode. The scan rate was 100 mVs^{-1} and solution of tetrabutylammonium hexafluorophosphate ($TBAPF_6$) in dichloromethane (0.1 M) was used as supporting electrolyte. E_g = HOMO-LUMO gap as calculated by at B3LYP/6-31G** level for C, H and N; and at Lanl2DZ level for Fe.

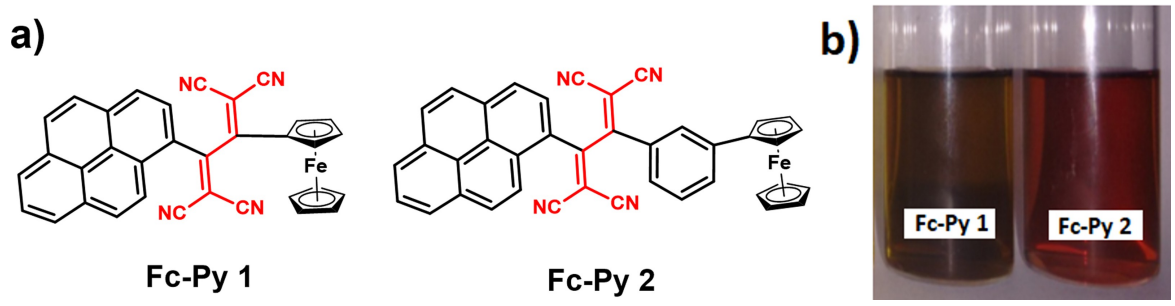

Figure 16. a) Chemical structures and b) colored photograph ($10^{<M->4}$M) of **Fc–Py 1** and **Fc–Py 2** in dichloromethane solution in day light. Figure reproduced from Reference 71.

Table 9. Photophysical, electrochemical and computational properties of **Fc–Py1** and **Fc–Py2**.

Pyrene	λ_{abs} (nm) [$\varepsilon/10^4$ ($M^{-1}cm^{-1}$)]	E^3 Ox (V)	E^2 Ox (V)	E^1 Ox (V)	E^1 Red (V)	E^2 Red (V)	E^3 Red (V)	E^4 Red (V)	E_g (eV)
Fc–Py1	639 [0.7], 474 [2.7]	1.35	1.18	0.45	−0.82	−1.18	−1.31	−1.84	2.54
Fc–Py2	483 [0.4]	–	1.15	0.08	−0.61	−1.12	−1.34	−1.82	1.89

E_g = HOMO-LUMO gap as calculated by DFT at B3LYP/6-31G** level for C, H and N; and at Lanl2DZ level for Fe; Potentials (V) measured versus Saturated Calomel Electrode (SCE) and referenced against FcH/FcH^+. (Recorded in dichloromethane solvent using tetrabutylammoniumhexafluorophosphate (Bu_4NPF_6) as supporting electrolyte at room temperature on a CHI620D electrochemical analyzer using Glassy carbon as working electrode, Pt wire as the counter electrode, and Saturated Calomel Electrode (SCE) as the reference electrode).

Fc–Py 2 exhibits two charge transfer bands; one is a strong charge transfer from pyrene moiety to the TCBD unit at 483 nm, and the second one is a weak charge transfer band from the ferrocenyl donor to the TCBD acceptor unit.

The electrochemical properties of mono-TCBD bridged pyrenes **Fc–Py 1** and **2** were investigated by cyclic voltammetry (CV) and differential pulse voltammetry (DPV) (Figure 17). **Fc–Py 1** exhibited three oxidation waves and **Fc–Py 2** showed two oxidation waves. The presence of electron deficient TCBD unit show low ferrocenyl oxidation at 0.45 V and 0.07 V for **Fc–Py 1** and **Fc–Py 2** respectively. The *meta* linkage at the phenyl moiety connected with ferrocene and TCBD hinders the electronic communication in **Fc–Py 2**. **Fc–Py 1** and **Fc–Py 2** exhibit two reduction waves corresponding to the mono-anion and di-anion formation at the TCBD unit.

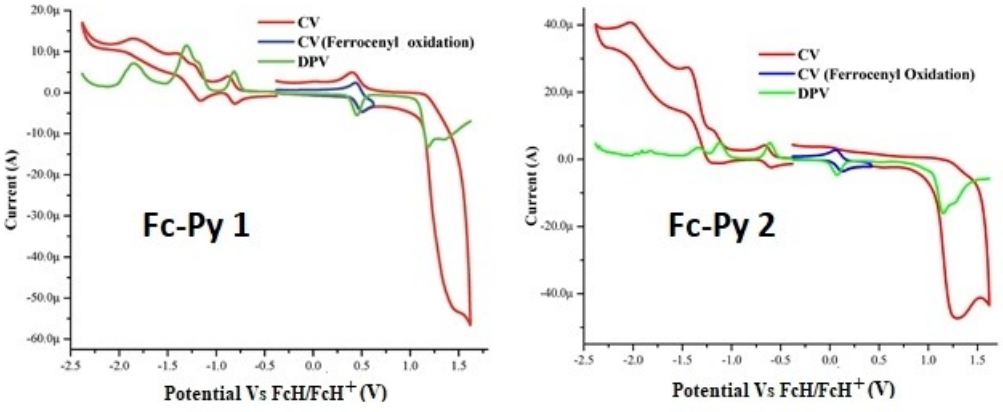

Figure 17. CV and DPV plots of pyrene based TCBD derivatives **Fc–Py 1** and **Fc–Py 2**. Figure reproduced from Reference 71.

1.10. Thiazole and Bisthiazole Based TCBD Derivatives

Thiazole and bisthiazole are electron acceptor units used for the design of π-conjugated donor-acceptor architectures.[72] The ferrocenyl TCBD derivatives of thiazole **Tz 1** and **Tz 2** (Figure 18) were synthesized by the CA-RE reaction sequence with electron rich triple bonds in 82% and 70% yield, respectively.[73] In the formation of thiazole **Tz 2**, the triple bond next to the ferrocene moiety *i. e.* the electron rich triple bond reacted with TCNE, while the other triple bond next to the thiazole moiety remained intact. The photophysical and electrochemical properties indicated that the incorporation of the TCBD moiety unit increased the molar absorption coefficient (ε) value of $\pi \rightarrow \pi^*$ transitions in **Tz 1** and **Tz 2**. The presence of a thiazole group adjacent to TCBD facilitates its reduction. The presence of an additional 4-ethynylphenyl spacer in **Tz 2** caused a red shifted absorption by 30 nm corresponding to a lower HOMO-LUMO gap. The TCBD derivatives **Tz 1** and **Tz 2** showed red shifted absorption towards NIR region with strong charge transfer bands, which indicated good electronic communication from electron donor to electron acceptor units. The thermoanalysis (TGA) showed that the incorporation of the TCBD unit enhances the thermal stability of ferrocenyl thiazoles.

The ethynyl linked ferrocenyl and triphenylamine bisthiazoles undergo CA-RE reaction sequence with two equivalents of TCNE, resulting in the formation of **Btz 1** and **Btz 2** in 71% and 65% yield, respectively (Figure 18).[74] The ferrocenyl and triphenylamine functionalized bisthiazoles upon reaction with TCNE afford TCBD derivatives, however, an attempt to synthesize the TCBD derivatives of the naphthalimide-functionalized bisthiazoles was unsuccessful. The reaction was further investigated by DFT calculations performed at B3LYP/6-31G** level for C, H and N, and at Lanl2DZ level for Fe, which reveal that the donor functionalized bisthiazoles favour the reaction with TCNE due to a lower HOMO-LUMO gap; on the other hand, acceptor functionalized bisthiazoles disfavour the reaction because of their large HOMO-LUMO gap. The photophysical and electrochemical properties of di-TCBD bridged symmetrical bisthiazoles **Btz 1** and **Btz 2** with ferrocenyl and triphenylamine end capping groups reveal strong donor-acceptor interactions.

The effect of the change in end capping group on the photophysical and electrochemical properties of bisthiazole reveals that the triphenylamine based **Btz 2** shows red shifted absorption and an easier reduction than that of ferrocenyl based **Btz 1** (Table 10). The ferrocenyl based **Btz 1** shows a less intense absorption band in the longer wavelength region related to a *d-d* transition of the ferrocenyl moiety. The oxidation of ferrocenyl based **Btz 1** was easier compared to triphenylamine based **Btz 2**. Thermogravimetric analysis indicated higher thermal stability in case of ferrocenyl substituted TCBD bridged thiazole and bisthiazole derivatives.

1.11. Comparison in di-(TPA-TCBD) Substituted Derivatives

The photophysical and electrochemical properties of di-(TPA-TCBD) substituted derivatives of DPP, isoindigo, BTD, phenothiazine and bisthiazole are shown in Table 11. The photophysical data show the di-(TPA-TCBD) substituted derivative of DPP central core show red shifted absorption than other derivatives with different central core as shown in figure 19 below.

The TCBD derivative with DPP central core **DPP 11** show absorption maximum towards near-infrared region

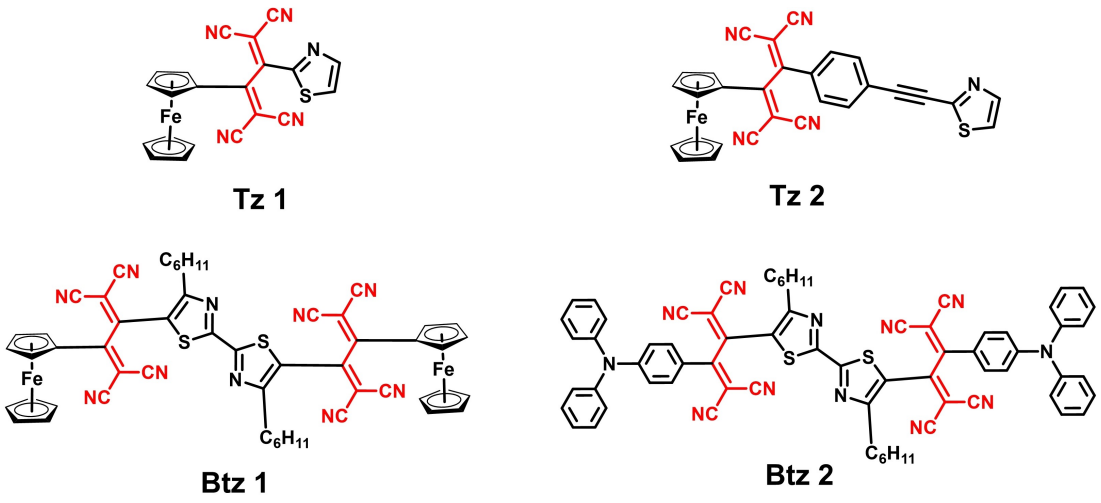

Figure 18. Chemical structures of TCBD bridged thiazole and bisthiazoles.

Table 10. Photophysical, thermal and electrochemical properties of TCBD linked thiazoles and bithiazoles.

	λ_{abs} (nm) [$\varepsilon/10^4$ ($M^{-1}cm^{-1}$)]	E^1 Ox (V)	E^1 Red (V)	E^2 Red (V)	E_g (eV)	T_d (°C)
Tz 1	600 [4.4]	0.84	−0.44	−0.75	3.49	336
Tz 2	630 [4.0]	0.85	−0.48	−0.80	3.45	443
Btz 1	356 [7.7]	0.38	−0.89	−1.45	1.94	307
Btz 2	457	0.82	−0.49	−1.01	1.74	293

E_g = HOMO-LUMO gap as calculated by DFT at B3LYP/6-31G** level for C, H and N, and at Lanl2DZ level for Fe; T_d = thermal decomposition temperature (TGA); Potentials measured versus Saturated Calomel Electrode (SCE) and referenced against FcH/FcH^+. Glassy carbon was used as working electrode, saturated calomel electrode (SCE) as the reference electrode and Pt wire as the counter electrode. The scan rate was 100 mVs^{-1} and solution of tetrabutylammonium hexafluorophosphate ($TBAPF_6$) in dichloromethane (0.1 M) was used as supporting electrolyte.

whereas other derivatives (**isoindigo 2, BTD 9, Phen 5 and Btz 2**) exhibit absorption maxima in visible region in between 460 nm to 500 nm. This red shifted absorption in TCBD bridged **DPP 11** was corresponds to the absorption of central DPP core and charge transfer from triphenylamine to TCBD and DPP. The electrochemical studies recorded with CV and DPV indicated the higher oxidation potential in **DPP 11** compared to other triphenylamine based TCBD derivatives (**isoindigo 2, BTD 9, Phen 5 and Btz 2**). The low reduction potential in DPP (**DPP11**), isoindigo (**isoindigo 2**), BTD (**BTD 9**) and bisthiazole (**Btz 2**) than that of phenothiazine (**phen 5**) is related to the presence of electron withdrawing moieties in the molecular structure.

E_g = HOMO-LUMO gap as calculated from electrochemical data (CV); Potentials (V) measured *versus* Ag/Ag+ electrode and referenced against FcH/FcH^+, Cyclic voltammograms and differential pulse voltammograms were recorded in dichloromethane solvent using glassy carbon as working

Table 11. Photophysical, electrochemical and computaional properties of di-(TPA-TCBD) substituted derivatives.

DPP	λ_{abs} (nm) [$\varepsilon/10^4$ ($M^{-1}cm^{-1}$)]	E^2 Ox (V)	E^1 Ox (V)	E^1 Red (V)	E^2 Red (V)	E^3 Red (V)	E^4 Red (V)	E_g (eV)
DPP 11	738 [1.9]	1.41	0.90	−0.59	−1.04	−1.26	1.90	1.49
Isoindigo 2	475 [5.6]	–	0.57	−1.16	−1.26	−1.27	–	1.95
BTD 9	490 [6.0]	–	0.64	−0.55	−0.70	−1.36	–	2.03
Phen 5	492 [4.0]	–	0.70	−0.92	−1.27	–	–	2.37
Btz 2	457	–	0.82	−0.49	−1.01	–	–	1.74

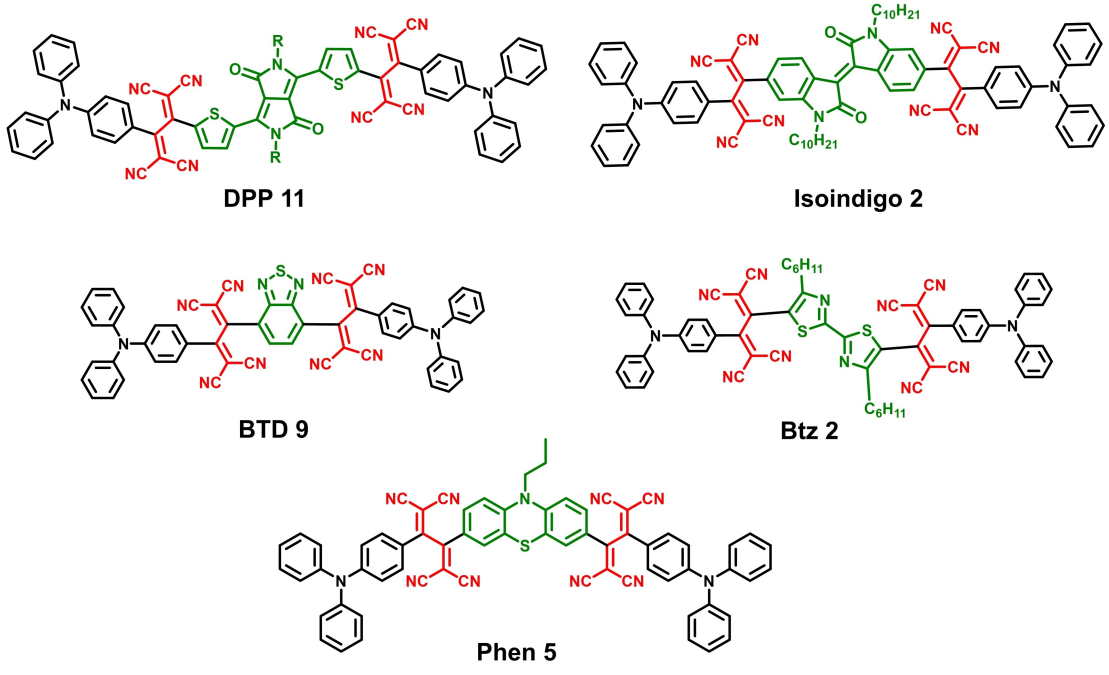

Figure 19. Chemical structure of TCBD bridged derivatives.

electrode, Pt wire as the counter electrode. The scan rate was 100 mVs^{-1}. A solution of tetrabutylammonium hexafluorophosphate ($TBAPF_6$) in dichloromethane (0.1 M) was used as supporting electrolyte.

2. Applications of TCBD Bridged Molecular Architectures

2.1. Solar Cells

Recently organic solar cells (OSCs) have gained the attention of researchers because of their simple device structure, easy fabrication, light weight and low production cost.[75–77]

2.1.1. Dye sensitized Solar Cells (DSSC)

Dye sensitized solar cells represent an emerging third-generation of solar cells attracting considerable attention due to their low manufacturing cost, flexibility and environmental compatibility.[78] After the first report in 1991 by Regan and Grätzel, significant research efforts have been devoted towards the development of efficient materials with efficiencies above 12%.[79] In spite of these advantages the main issue with recently reported results is the stability of the devices, which limits their use as low-cost DSSC in the market.

The di-TCBD bridged ferrocenyl substituted triphenylamine **TPA9** (Figure 20) was used as sensitizer for DSSCs. The devices based on **TPA9** show a higher power conversion efficiency of 4.96% compared to its precursor **D1** (3.65%). The higher power conversion efficiency for **TPA9** was attributed to the increase in the light harvesting property of dye **TPA9** due to its extended absorption in the near infrared region.[80]

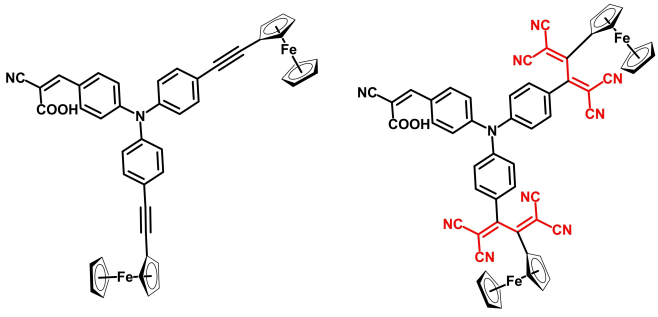

D1 **TPA9**

Figure 20. Chemical structures of ethyne bridged **D1** and TCBD bridged **TPA9**.

2.1.2. Bulk Heterojunction Organic Solar Cells

2.1.2.1. TCBD Bridged Derivatives as Donors

The triphenylamine based TCBD bridged molecular architectures have been used for organic solar cells.[81] By varying the end group on BTD moiety, **BTDs 3**, **5** and **6** (Figure 15) have been used as donors along with the fullerene derivative [6,6]-phenyl-C_{71}-butyric acid methyl ester ($PC_{71}BM$), as an acceptor for bulk heterojunction organic solar cells.

In order to improve the device performance, the end capping donor group was varied while keeping the triphenylamine-TCBD based benzothiadiazole as the constant moiety (Figure 15). The carbazole substituted benzothiadiazole with TCBD linker **BTD3** was employed as the donor component for bulk heterojunction organic solar cells along with $PC_{71}BM$ as the electron acceptor, which resulted in a power conversion efficiency of 2.76%.[82] Further, by the use of various end capping groups in BTD based molecular systems such as 3-pyridyl[83] **BTD5** and 9-anthracenyl[84] **BTD6**, the power conversion efficiency was improved. The anthracene functionalized BTD **BTD6** with an ethynyl bridge achieved a power conversion efficiency of up to 4.61% (Table 12).

Blanchard *et al.* synthesized symmetrical and unsymmetrical TCBD bridged push-pull derivatives (**TPA-Ds 1–3**, Figure 21) with increase in thiophene moieties. These systems showed good solubility in common organic solvents and high stability. **TPA-Ds 1–3** exhibit strong absorption in the visible region, high oxidation potentials. The optical and electrochemical investigations indicated these push-pull derivatives can be used as donor material for bilayer heterojunction solar cells. The average power conversion efficiency of 1.05% was recorded from analysis of four different cells. The best efficiency was observed for the device with power conversion efficiency of 1.08% with current density of 3.06 $mA\,cm^{-2}$, FF = 0.33and an open-circuit voltage 0.97 V.

Later in 2021, Blanchard *et al.* reported triphenylamine based tetracyanobutadiene molecular systems end-capped with

Table 12. Photovoltaic parameters of TCBD bridged donor **BTDs 3**, **5** and **6** under optimized conditions along with fullerene derivative $PC_{71}BM$ as an acceptor.

Active layer	J_{sc} (mA/cm^2)	V_{oc} (V)	FF	PCE (%)
BTD3[a]	7.56	0.96	0.38	2.76
BTD5[b]	6.34	0.98	0.36	2.24
BTD5[c]	9.84	0.94	0.58	5.36
BTD6[d]	7.45	0.94	0.45	3.15
BTD6[e]	9.48	0.90	0.54	4.61

[a]Processed from DCM; [b]as cast from chloroform; [c]two step annealing; [d]processed with THF; [e]processed with chloronaphthalene (CN) (3vol.%)/THF, PCE=Power conversion efficiency, J_{sc} = current density, V_{oc} = open circuit voltage, FF = fill factor.

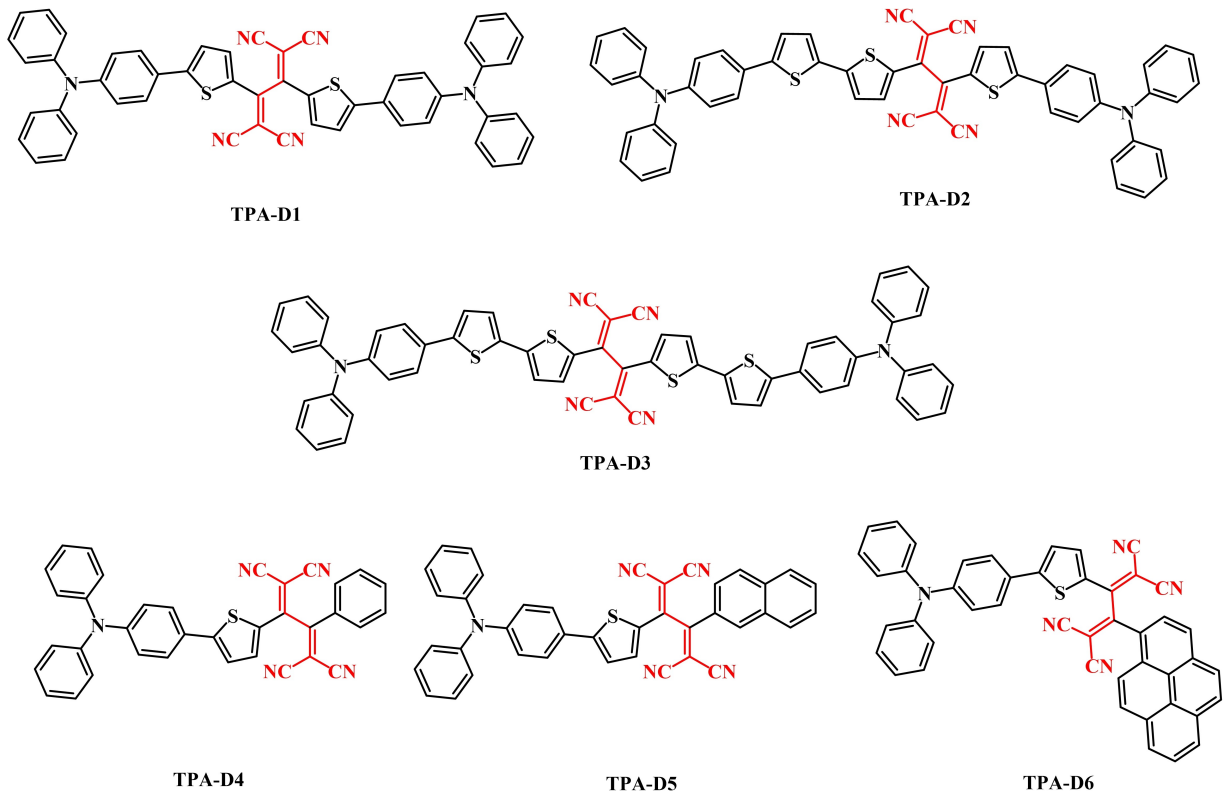

Figure 21. Chemical structures of the TCBD linked derivatives **TPA-D 1–6** for organic solar cells.

aryl group of increasing conjugation; phenyl (**TPA-D4**), naphthyl (**TPA-D5**) and pyrenyl (**TPA-D6**) (Figure 21).[85] They explored their photophysical properties which show broad absorption spectra covering visible region from 300 nm to 800 nm with two absorption bands low energy charge transfer and high energy π-π^* transition. The temperature dependent (10–70 °C), UV-vis absorption studies were performed, which reveals absence of aggregation in the solution state. The **TPA-Ds 4–6** were non-emissive in the solution state, however it was found to be emissive in the thin films with emission maxima 760–780 nm and PMMA matrix with emission maxima 653–665 nm, which is due to restricted intramolecular rotation. The red shift in the emission in thin film sate is due to π-π intermolecular interactions. The optical properties indicated the suitability of **TPA-Ds 4–6** to use these materials as donor for organic solar cells. **TPA-Ds 4–6** were used as donor in all vacuum-processed planar hetero-junction (PHJ) solar cell and it was observed that the PCE values were inversely proportional to the thickness of the donor layers. The PCE values revealed that smaller aromatic substituents show better performance than the larger once. The phenyl derivative **TPA-D4** (PCE = 1.86 %) showed better performance than naphthalene **TPA-D5** (PCE = 1.23 %) and pyrene **TPA-D6** (PCE = 0.96 %).

2.1.2.2. TCBD Linked Derivatives as a Non-Fullerene Acceptor

Fullerene derivatives [6,6]-phenyl-C_{61}-butyric acid methyl ester ($PC_{61}BM$) and [6,6]-Phenyl C_{71} butyric acid methyl ester ($PC_{71}BM$) are commonly used as electron acceptor materials for bulk heterojunction organic solar cells because of their excellent electron acceptor properties.[86] During the last two decades a drastic improvement in the performance of donor materials for solar cells has been observed,[87–88] however, the development of acceptor materials lagged behind. Recently various design strategies and the optimization of processes significantly enhanced the performance of non-fullerene acceptors.[89–90]

The introduction of TCBD in a molecular system improves the acceptor strength of the resulting compound and lowers the HOMO and LUMO energy levels.[91] The use of TCBD derivatives as donors in bulk heterojunction organic solar cells is well known in the literature,[82–84] however, the incorporation of TCBD in donor functionalized diketopyrrolopyrroles (DPP) improves their acceptor strength. The DPP molecules containing a TCBD bridge with improved acceptor strengths exhibit energy levels, which match with the polymer donor (Figure 22), thereby indicating that they can be used as

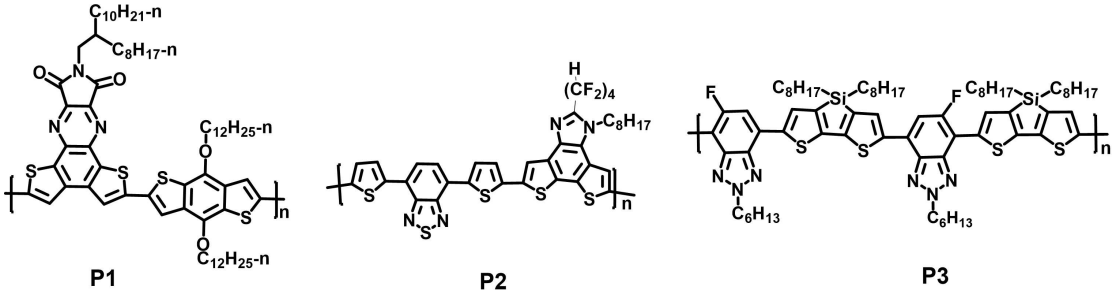

Figure 22. Chemical Structures of different polymer donors used in solar cells.

non-fullerene acceptors for bulk heterojunction organic solar cells.

When triphenylamine substituted mono- and di-TCBD bridged DPP materials (**DPP**s **2** and **11**, Figure 23) were used as non-fullerene acceptors along with polymer donor **P1**, they showed an overall power conversion efficiency of 1.16% and 1.57%, respectively.[43a] By solvent vapor annealing the power conversion efficiency was significantly improved up to 3.90% and 4.95% for **P1**:**DPP2** and **P1**:**DPP11**, respectively.

The ferrocenyl substituted TCBD bridged **DPP**s **1** and **10**, (Figure 7 and 23) were used as non-fullerene acceptors along with the polymer donor **P2**, showed an overall power conversion efficiency of 1.16% and 1.57%, respectively.[92] The solvent additive treatment with 3 vol% 1,8-diiodoctane was employed to enhance the performance and power conversion efficiencies up to 4.23% and 4.88%, for **P2**:**DPP1** and **P2**:**DPP10**, respectively, were observed. Thermal annealing and vacuum dried films were applied to further improve the performance, and with vacuum dried films **P2**:**DPP1** and **P2**:**DPP10** maximum power conversion efficiencies of up to 6.44% and 6.89% were obtained, respectively.

The mono-TCBD bridged *N*-phenyl carbazole functionalized DPPs (**DPP**s **3** and **7**, Figure 23) were used as non-fullerene solar cells along with polymer donor **P3**, and the devices based on optimized **P3**:**DPP3** and **P3**:**DPP7** active layers showed maximum power conversion efficiencies of 4.86% and 7.19%, respectively, which shows that the use of an additional ethynyl linked *N*-phenyl carbazole unit significantly improved the performance.[93] The systematic change in the end capping donors (triphenylamine, *N*-phenyl carbazole

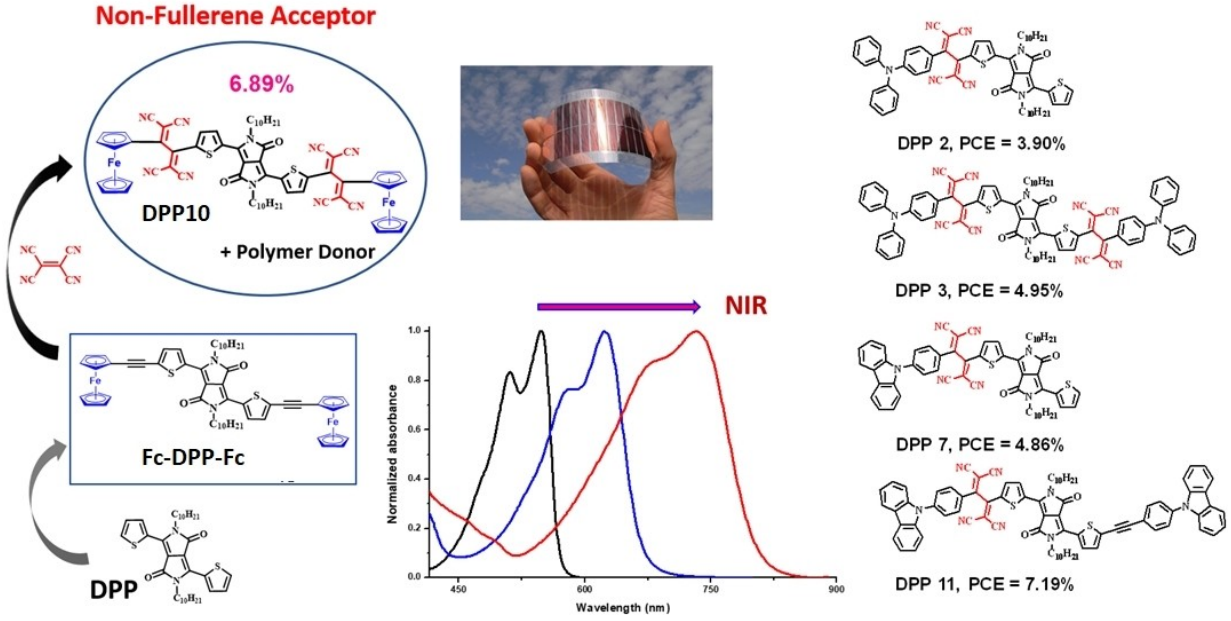

Figure 23. Development of TCBD linked DPP acceptors for organic solar cells. (OSCs picture source: https://www.ise.fraunhofer.de/en/business-areas/photovoltaics/perovskite-and-organic-photovoltaics/organic-solar-cells-and-modules.html)

and ferrocene) varies the performance of non-fullerene acceptors. The *N*-phenyl carbazole based devices showed better performance and realized power conversion efficiency of 7.19% (for **DPP7**) which is the respectable efficiency for TCBD based non-fullerene acceptors (Figure 23 and Table 13). Thereby, the use of TCBD as non-fullerene acceptor opened up a new direction to design efficient acceptor materials for OSCs.

Praveen *et al.* has reported mono- and di-TCBD derivatives of azulene,[94] carbazole,[95] and fluorene[95] as a non-fullerene acceptors for organic solar cells (Figure 24). The di-TCBD based derivatives exhibit red shifted absorption, better aggregation behavior and low HOMO-LUMO gap compared to mono-TCBD bridged derivatives which indicated the potential of these molecules to use as a non-fullerene acceptors. When mono- and di-TCBD derivative of azulene **Az-NFA-1** and **Az-NFA-2** were used as non-fullerene acceptors along with P3HT donor showed PCEs of 1.04% and 1.70%. The better performance in di-TCBD bridged **Az-NFA-2** derivatives was related to strong electron accepting ability, deep LUMO level, high molar absorption coefficient.

The unsymmetrical and symmetrical non-fullerene acceptors made up of carbazole and fluorene were used along with the donor P3HT exhibited the PCEs in the range from 4 to 6.30%. When these acceptors used as-cast blend showed better performance (PCEs = 4.24–5.37%) compared to the prepared standard P3HT:PCBM device (4.14%). The symmetrical TCBD derivatives fabricated as-cast devices displayed better PCEs (**F-NFA2**, PCE = 5.37%; **Cz-NFA2**, PCE = 5.21%) compared to unsymmetrical TCBD derivatives (**F-NFA1**, PCE = 4.56%; **Cz-NFA1**, PCE = 4.24%). When the devices processed with additive 1,8-diiodooctane (DIO) improvement in the performance was observed and showed 6.30% (**Cz-NFA2**), 5.42%, (**F-NFA2**) 5.09% (**Cz-NFA1**), and 4.65% (**F-NFA1**) PCE, indicating the role of DOI in increasing the photocurrent. The higher efficiency in case of di-TCBD bridged derivatives is related to the broad red shifted absorption and more number of cyano groups which improved the acceptor strength of the molecule.

Table 13. Photovoltaic parameters of DPP based acceptors blended with polymers **P1**–**P3** as electron donors.

Active layer	J_{sc} (mA/cm^2)	V_{oc} (V)	FF	PCE (%)
DPP 1[c]	10.52	0.98	0.52	5.36
DPP 1[d]	11.34	0.98	0.58	6.44
DPP 2[a]	3.88	0.88	0.34	1.16
DPP 2[b]	8.15	0.92	0.52	3.90
DPP 3[a]	7.43	0.98	0.39	2.84
DPP 3[b]	10.56	0.94	0.49	4.86
DPP 7[a]	9.25	0.94	0.45	3.91
DPP 7[b]	13.78	0.90	0.58	7.19
DPP 10[c]	11.86	0.88	0.55	5.74
DPP 10[d]	12.66	0.88	0.62	6.89
DPP 11[a]	5.82	0.82	0.38	1.57
DPP 11[b]	10.28	0.86	0.56	4.95

[a]cast from THF; [b]solvent vapor annealing; [c]thermal annealing; vacuum dried; [c] solvent annealing; PCE=Power conversion efficiency, J_{sc} = current density, V_{oc} = open circuit voltage, FF = fill factor.

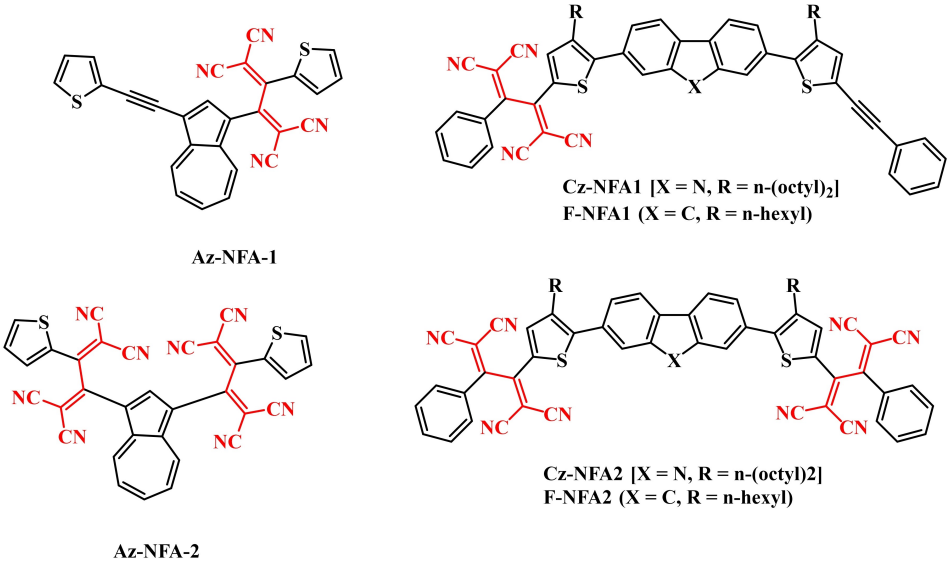

Figure 24. Chemical structures of TCBD linked non-fullerene acceptors for organic solar cells.

2.2. Photothermal Therapy (for Cancer Treatment)

The photothermal therapy (PTT) for cancer treatment has gained attention of the scientific community as it is a highly selective and noninvasive therapeutic method by the use of NIR laser-induced ablation of tumor cells.[96–97]

Dong *et al.* reported donor-acceptor (D–A) triphenylamine based furan, thiophene, and selenophene functionalized DPPs for photothermal cancer therapy,[98–99] which showed promising performance as therapeutic agents for photothermal therapy. The triphenylamine based furan, thiophene, and selenophene functionalized DPPs used for photothermal cancer therapy, showed photothermal conversion efficiency (PTC) of 47%, 34.5% and 37.9%, respectively. This indicates that the furan functionalized DPP has shown higher photothermal conversion efficiency than the other thiophene and selenophene functionalized DPPs.

In order to further improve the PTC efficiency, the authors selected furan functionalized DPP over thiophene functionalized DPP, because the steric hindrance of furyl-DPP is smaller than that of thienyl-DPP resulting in better co-planarity. Another component is ferrocene, which itself is a cancer therapeutic agent[100] and a good electron donor helping in fluorescence quenching and singlet-oxygen production *via* a photo-induced electron transfer (PET) process, which enhances non radiative transition. It has also been reported that nanoparticles containing iron are useful in applications for photothermal therapy.[101] The TCBD moiety was selected due to its strong electron withdrawing nature, and its incorporation into push-pull systems shows a red shift in the electronic absorption in NIR region and can promote the PET process. Use of the designed molecule **DPPCN-Fc** (Figure 25) as cancer theranostic agent for cancer therapy achieved 59.1% of PTC efficiency, which is higher compared to earlier reported DPPs.[7b]

3. Summary, Conclusion and Future Outlook

In this review we have highlighted the design strategies used for the synthesis of various TCBD linked donor-acceptor derivatives by the click type CA-RE reaction sequence. The photophysical and electrochemical properties of TCBD derivatives based on DPP, isoindigo, BTD, pyrene, pyrazabole, truxene, BODIPY, phenothiazine, triphenylamine, and bisthiazole have been described. Further, we have highlighted the important emerging applications of TCBD derivatives in dye sensitized solar cells, bulk heterojunction organic solar cells and photothermal cancer therapy.

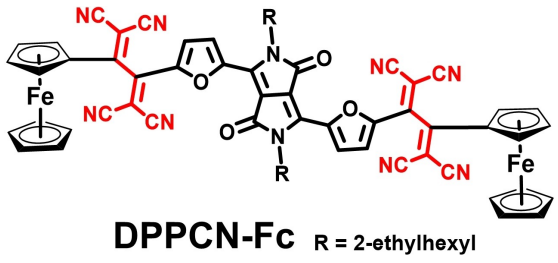

Figure 25. Chemical structure of TCBD bridged **DPPCN-Fc**.

4. Some Conclusions to be Drawn from this Review are the Following

a. The effect of incorporation of the first TCBD is more pronounced compared to the second and third TCBD incorporations in terms of absorption and electrochemical changes. The incorporation of the first TCBD exhibits a huge red shift in the electronic absorption spectra compared to second/third TCBD incorporations.
b. Incorporation of TCBD is more effective when TCBD is the only acceptor in the molecular architecture. The effect of TCBD incorporation is less effective, when another acceptor moiety is already present in molecular architecture.
c. As the number of TCBD units increases in the molecule, it shows a red shift in absorption along with a decrease in band gap linearly.
d. In some cases, TCBD incorporation shifts the absorption from the UV to the Vis region (pyrazabole) as well as from the Vis to the NIR region (DPP).
e. The incorporation of end capping donors and TCBD (acceptor) on both sides of the building block improved the absorption and the acceptor strength with a decrease in band gap, which exhibited better photovoltaic performance compared to substitution of end capping donor and TCBD (acceptor) on only one side.
f. The TCBD incorporation improves the donor-acceptor interaction leading to an improvement in the absorption with a lowering of the band gap.
g. The electrochemical study reveals that the oxidation of ferrocenyl based TCBD derivatives is easier compared to the oxidation of triphenylamine based TCBD derivatives, whereas the reduction of triphenylamine based TCBD derivatives is easier compared to the ferrocenyl based TCBD derivatives.
h. TCBD incorporation improves the acceptor strength of a molecule, and in the case of DPP based TCBD derivatives it was observed that the di-TCBD bridged DPPs exhibit better photovoltaic performance than their mono-TCBD bridged analogues.

i. The TCBD derivatives with a triphenylamine donor show red shifted broad absorption compared to other end capping donors.
j. The carbazole based TCBD derivatives show higher power conversion efficiency compared to other donor based TCBD derivatives.

The analysis of parameters for the TCBD bridged derivatives discussed in this review shows that by selecting the core with absorption in the visible region, one can extend the absorption towards the NIR region by substitution of appropriate donor and TCBD with a decrease in HOMO-LUMO gap. The derivatives with NIR absorption and low HOMO-LUMO gap are of great interest for OSCs and photothermal therapy applications. This review provides a new direction for the design of highly efficient donor-acceptor architectures for photovoltaic and biomedical applications.

Acknowledgements

We thank the and SERB (Project No. CRG/2018/000032), New Delhi, and DAAD *New Passage to India* (Leibniz University Hannover and IIT Indore project). R. M. thanks the Alexander von Humboldt Foundation for a research fellowship. Open Access funding enabled and organized by Projekt DEAL.

References

[1] a) N. Kobayashi, S. Inagaki, V. N. Nemykin, T. Nonomura, *Angew. Chem. Int. Ed.* **2001**, *40*, 2710–2712; *Angew. Chem.* **2001**, *113*, 2782–2784; b) C. Ji, L. Yin, K. Li, L. Wang, X. Jiang, Y. Suna, Y. Li, *RSC Adv.* **2015**, *5*, 31606–31614; c) W. Y. Wong, W. K. Wong, P. R. Raithby, *J. Chem. Soc. Dalton Trans.* **1998**, 2761–2766.

[2] a) Y. Patil, R. Misra, *Chem. Rec.* **2018**, *18*, 1350–1364; b) Y. Patil, R. Misra, *Chem. Asian J.* **2018**, *13*, 220–229; c) Y. Patil, R. Misra, *J. Mater. Chem. C* **2019**, *7*, 42, 13020–13031.

[3] a) H. Liu, H. Jia, L. Wang, Y. Wu, C. Zhan, H. Fu, J. Yao, *Phys. Chem. Chem. Phys.* **2012**, *14*, 14262–14269; b) Y. Patil, R. Misra, *Chem. Rec.* **2020**, *20*, 596–603; c) Y. Patil, R. Misra, A. Sharma, G. D. Sharma, *Phys. Chem. Chem. Phys.* **2016**, *18*, 25, 16950–16957.

[4] a) T. Michinobu, F. Diederich, *Angew. Chem. Int. Ed.* **2018**, *57*, 3552–3577; *Angew. Chem.* **2018**, *130*, 3612–3638; b) A. V. Muñoz, H. Gotfredsen, M. Jevric, A. Kadziola, O. Hammerich, M. B. Nielsen, *J. Org. Chem.* **2018**, *83*, 2227–2234.

[5] a) P. S. Rao, A. Gupta, S. V. Bhosale, A. Bilic, W. Xiang, R. A. Evans, S. V. Bhosale, *Dyes Pigm.* **2017**, *146*, 502–511; b) T. Michinobu, C. Boudon, J. P. Gisselbrecht, P. Seiler, B. Frank, N. N. P. Moonen, M. Gross, F. Diederich, *Chem. Eur. J.* **2006**, *12*, 1889–1905.

[6] a) A. R. Izzotti, J. L. Gleason, *Chem. Eur. J.* **2022**, 28, e202201418; b) L. M. Mateo, L. Sagresti, Y. Luo, D. M. Guldi, T. Torres, G. Brancato, G. Bottari, *Chem. Eur. J.* **2021**, *27*, 16049; c) C. Philippe, M. Coste, Y. Bretonnière, L. Lemiègre, S. Ulrich, Y. Trolez, *Eur. J. Org. Chem.* **2022**, e202200049; d) M. Rimmele, F. Glöcklhofer, M. Heeney, *Mater. Horiz.* **2022**, DOI: 10.1039/d2mh00519k ; e) T. Shoji, A. Maruyama, E. Shimomura, D. Nagai, S. Ito, T. Okujima, K. Toyota, *Eur. J. Org. Chem.* **2015**, *2015*, 1979–1990.

[7] a) N. Ripoche, M. Betou, C. Philippe, Y. Trolez, O. Mongin, M. Dudek, Z. Pokladek, K. Matczyszyn, M. Samoc, H. Sahnoune, J.-F. Halet, T. Roisnel, L. Toupet, M. Cordier, G. Moxey, M. G. Humphrey, F. Paul, *Phys. Chem. Chem. Phys.* **2021**, *23*, 22283–22297; b) P. Liang, Q. Tang, Y. Cai, G. Liu, W. Si, J. Shao, W. Huang, Q. Zhang, X. Dong, *Chem. Sci.* **2017**, *8*, 7457–7463; c) A. R. Izzotti, J. L. Gleason, *Chem. Eur. J.* **2022**, *28*, e202201418.

[8] a) B. Sekaran, A. Dawson, Y. Jang, K. V. MohanSingh, R. Misra, F. D'Souza, *Chem. Eur. J.* **2021**, *27*, 14335; b) J. Shinde, M. B. Thomas, M. Poddar, R. Misra, F. D'Souza, *J. Phys. Chem. C* **2021**, *125*, 23911–23921; c) T. Shoji, K. Miura, T. Araki, A. Maruyama, A. Ohta, R. Sekiguchi, S. Ito, T. Okujima, *J. Org. Chem.* **2018**, *83*, 6690–6705; d) T. Shoji, A. Maruyama, M. Tanaka, D. Nagai, E. Shimomura, K. Fujimori, S. Ito, T. Okujima, K. Toyota, M. Yasunami, *ChemistrySelect* **2016**, *1*, 49–56.

[9] a) A. T. Bui, C. Philippe, M. Beau, N. Richy, M. Cordier, T. Roisnel, L. Lemiègre, O. Mongin, F. Paul, Y. Trolez, *Chem. Commun.* **2020**, *56*, 3571–3574; b) K. Erden, C. Dengiz, *J. Org. Chem.* **2022**, *87*, 4385–4399; c) C. Philippe, A. T. Bui, M. Beau, H. Bloux, F. Riobé, O. Mongin, T. Roisnel, M. Cordier, F. Paul, L. Lemiègre, Y. Trolez, *Chem. Eur. J.* **2022**, *28*, e202200025; d) T. Shoji, M. Maruyama, A. Maruyama, D. Nagai, M. Tanaka, R. Sekiguchi, S. Ito, T. Okujima, *Heterocycles* **2017**, *95*, 353–369.

[10] a) C. Philippe, A. T. Bui, S. Batsongo-Boulingui, Z. Pokladek, K. Matczyszyn, O. Mongin, L. Lemiègre, F. Paul, T. A. Hamlin, Y. Trolez, *Org. Lett.* **2021**, *23*, 2007–2012; b) K. A. Winterfeld, G. Lavarda, K. Yoshida, M. J. Bayerlein, K. Kise, T. Tanaka, A. Osuka, D. M. Guldi, T. Torres, G. Bottari, *J. Am. Chem. Soc.* **2020**, *142*, 7920–7929.

[11] a) K. A. Winterfeld, G. Lavarda, J. Guilleme, D. M. Guldi, T. Torres, G. Bottari, *Chem. Sci.* **2019**, *10*, 10997–11005; b) Y. Rout, Y. Jang, H. B. Gobeze, R. Misra, F. D'Souza, *J. Phys. Chem. C* **2019**, *123*, 23382–23389.

[12] a) I. S. Yadav, Y. Jang, Y. Rout, M. B. Thomas, R. Misra, F. D'Souza, *Chem. Eur. J.* **2022**, *28*, e202200348; b) Y. Jang, Y. Rout, R. Misra, F. D'Souza, *J. Phys. Chem. B* **2021**, *125*, 4067–4075; c) I. S. Yadav, A. Z. Alsaleh, R. Misra, F. D'Souza, *Chem. Sci.* **2021**, *12*, 1109–1120.

[13] a) T. Shoji, S. Ito, K. Toyota, M. Yasunami, N. Morita, *Chem. Eur. J.* **2008**, *14*, 8398–8408; b) Y. Wu, M. C. Stuparu, C. Boudon, J. Gisselbrecht, W. B. Schweizer, K. K. Baldridge, J. S. Siegel, F. Diederich, *J. Org. Chem.* **2012**, *77*, 11014–11026.

[14] M. I. Bruce, J. R. Rodgers, M. R. Snow, A. G. Swincer, *J. Chem. Soc. Chem. Commun.* **1981**, 271–272.
[15] a) T. Michinobu, J. C. May, J. H. Lim, C. Boudon, J. Gisselbrecht, P. Seiler, M. Gross, I. Biaggio, F. Diederich, *Chem. Commun.* **2005**, 737–739; b) M. Kivala, C. Boudon, J. Gisselbrecht, P. Seiler, M. Gross, F. Diederich, *Chem. Commun.* **2007**, 4731–4733.
[16] a) M. Stefko, M. D. Tzirakis, B. Breiten, M. O. Ebert, O. Dumele, W. B. Schweizer, J. P. Gisselbrecht, C. Boudon, M. T. Beels, I. Biaggio, F. Diederich, *Chem. Eur. J.* **2013**, *19*, 12693–12704; b) M. Kivala, F. Diederich, *Acc. Chem. Res.* **2009**, *42*, 235–248; c) S. I. Kato, F. Diederich, *Chem. Commun.* **2010**, *46,* 1994–2006.
[17] a) T. Mochida, S. Yamazaki, *J. Chem. Soc. Dalton Trans.* **2002**, 3559; b) T. Michinobu, *Pure Appl. Chem.* **2010**, *82*, 1001–1009.
[18] a) M. Jordan, M. Kivala, C. Boudon, J.-P. Gisselbrecht, W. B. Schweizer, P. Seiler, F. Diederich, *Chem. Asian J.* **2011**, *6*, 396–401; b) T. Shoji, S. Ito, T. Okujima, N. Morita, *Eur. J. Org. Chem.* **2011**, 5134–5140.
[19] a) T. Shoji, S. Ito, T. Okujima, N. Morita, *Chem. Eur. J.* **2013**, *19*, 5721–5730; b) B. Breiten, M. Jordan, D. Taura, M. Zalibera, M. Griesser, D. Confortin, C. Boudon, J.-P. Gisselbrecht, W. B. Schweizer, G. Gescheidt, F. Diederich, *J. Org. Chem.* **2013**, *78*, 1760–1767.
[20] a) C. Dengiz, B. Breiten, J.-P. Gisselbrecht, C. Boudon, N. Trapp, W. B. Schweizer, F. Diederich, *J. Org. Chem.* **2015**, *80*, 882–896; b) N. Kraußе, M. Kielmann, J. Ma, H. Butenschön, *Eur. J. Org. Chem.* **2015**, 2622–2631.
[21] T. Shoji, A. Maruyama, C. Yaku, N. Kamata, S. Ito, T. Okujima, K. Toyota, *Chem. Eur. J.* **2015**, *21*, 402–409.
[22] a) M. I. Bruce, F. de Montigny, M. Jevric, C. Lapinte, B. W. Skelton, M. E. Smith, A. H. White, *J. Organomet. Chem.* **2004**, *689*, 2860–2871; b) M. I. Bruce, P. J. Low, F. Hartl, P. A. Humphrey, F. de Montigny, M. Jevric, C. Lapinte, G. J. Perkins, R. L. Roberts, B. W. Skelton, A. H. White, *Organometallics* **2005**, *24*, 5241–5255.
[23] a) T. Shoji, E. Shimomura, M. Maruyama, A. Maruyama, S. Ito, T. Okujima, K. Toyota, N. Morita, *Eur. J. Org. Chem.* **2013**, 7785–7799; b) T. Michinobu, N. Satoh, J. Cai, Y. Lia, L. Han, *J. Mater. Chem. C* **2014**, *2*, 3367–3372.
[24] a) Y. Yuan, T. Michinobu, N. Satoh, M. Ashizawa, L. Han, *J. Nanosci. Nanotechnol.* **2015**, *15*, 5856–5866; b) T. Shoji, N. Kamata, A. Maruyama, S. Ito, T. Okujima, *Bull. Chem. Soc. Jpn.* **2015**, *88*, 1338–1346.
[25] a) T. Michinobu, H. Kumazawa, K. Noguchi, K. Shigehara, *Macromolecules* **2009**, *42*, 5903–5905; b) R. Misra, P. Gautam, S. M. Mobin, *J. Org. Chem.* **2013**, *78*, 12440–12452.
[26] a) X. Tang, W. Liu, J. Wu, C.-S. Lee, J. You, P. Wang, *J. Org. Chem.* **2010**, *75*, 7273–7278; b) B. H. Tchitchanov, M. Chiu, M. Jordan, M. Kivala, W. B. Schweizer, F. Diederich, *Eur. J. Org. Chem.* **2013**, 3729–3740.
[27] a) Ivan, T. Vacareanu, L. Grigoras, *M. Rev. Chim. (Bucharest, Rom.)* **2013**, *64*, 372–377; b) M. Betou, N. Kerisit, E. Meledje, Y. R. Leroux, C. Katan, J.-F. Halet, J.-C. Guillemin, Y. Trolez, *Chem. Eur. J.* **2014**, *20*, 9553–9557.
[28] Z. Pokladek, N. Ripoche, M. Betou, Y. Trolez, O. Mongin, J. Olesiak-Banska, K. Matczyszyn, M. Samoc, M. G. Humphrey, M. Blanchard-Desce, F. Paul, *Chem. Eur. J.* **2016**, *22*, 10155–10167.
[29] a) J. Grolleau, F. Gohier, M. Allain, S. Legoupy, C. Cabanetos, P. Frère, *Org. Electron.* **2017**, *42*, 322–328; b) Y. Gu, X. Zhou, Y. Li, K. Wu, F. Wang, M. Huang, F. Guo, Y. Wang, S. Gong, D. Ma, C. Yang, *Org. Electron.* **2015**, *25*, 193–199.
[30] a) M. Can, M. Z. Yigit, K. Seintis, D. Karageorgopoulos, S. Demic, S. Icli, V. Giannetas, M. Fakis, E. Stathatos, *Synth. Met.* **2014**, *188*, 77–85; b) M.-B. Madec, J. J. Morrison, M. Rabjohns, M. L. Turner, S. G. Yeates, *Org. Electron.* **2010**, *11*, 686–691.
[31] R. Misra, R. Maragani, P. Gautam, S. M. Mobin, *Tetrahedron Lett.* **2014**, *55*, 7102–7105.
[32] R. Misra, R. Maragani, *Tetrahedron* **2014**, *70*, 3390–3399.
[33] a) T. Jadhav, R. Maragani, R. Misra, V. Sreeramulu, D. N. Rao, S. M. Mobin, *Dalton Trans.* **2013**, 4340–4342; b) T. Jadhav, B. Dhokale, Y. Patil, R. Misra, *RSC Adv.* **2015**, *5*, 68187–68191.
[34] a) A. Hayek, F. Bolze, C. Bourgogne, P. L. Baldeck, P. Didier, Y. Arntz, Y. Mely, J. F. Nicoud, *Inorg. Chem.* **2009**, *48*, 9112–9119; b) Z. M. Hudson, S. Wang, *Acc. Chem. Res.* **2009**, *42*, 1584; c) F. Jakle, *Chem. Rev.* **2010**, *110*, 3985–4022.
[35] a) Y. Patil, R. Misra, *J. Organomet. Chem.* **2017**, *840*, 23–29; b) Y. Patil, T. Jadhav, B. Dhokale, H. Butenschön, R. Misra, *ChemistrySelect* **2017**, *2*, 415–420.
[36] S. Diring, R. Ziessel, *Tetrahedron Lett.* **2009**, *50*, 1203–1208.
[37] a) B. Ventura, A. Barbieri, F. Barigelletti, S. E. Diring, R. Ziessel, *Inorg. Chem.* **2010**, *49*, 8333–8346; b) F. Goubard, F. Dumur, *RSC Adv.* **2015**, *5*, 3521–3551; c) M. M. Boorum, Y. V. Vasil, T. Drewello, L. T. Scott, *Science* **2001**, *294*, 828–831.
[38] a) P. W. Rabideau, A. H. Abdourazak, Z. Marcinow, R. Sygula, A. Sygula, *J. Am. Chem. Soc.* **1995**, *117*, 6410–6411; b) X. Zong, M. Liang, C. Fan, K. Tang, G. Li, Z. Sun, S. Xue, *J. Phys. Chem. C* **2012**, *116*, 11241–11250; c) Y. Xie, X. Zhang, Y. Xiao, Y. Zhang, F. Zhou, J. Qib, J. Qu, *Chem. Commun.* **2012**, *48*, 4338–4340.
[39] a) H. J. Xua, B. Dub, C. P. Gros, P. Richarda, J. M. Barbea, D. H. Pierre, *J. Porphyrins Phthalocyanines* **2013**, *17*, 44–55; b) M. Kimura, S. Kuwano, Y. Sawaki, H. Fujikawa, K. Noda, Y. Taga, K. Takagi, *J. Mater. Chem.* **2005**, *15*, 2393–2398.
[40] a) R. Sharma, M. B. Thomas, R. Misra, F. D'Souza, *Angew. Chem. Int. Ed.* **2019**, *58*, 4350–4355; *Angew. Chem.* **2019**, *131*, 4394–4399; b) R. Sharma, R. Maragani, R. Misra, *New J. Chem.* **2018**, *42*, 882–890; c) R. Misra, R. Sharma, S. M. Mobin, *Dalton Trans.* **2014**, *43*, 6891–6896.
[41] a) M. Grzybowski, D. T. Gryko, *Adv. Opt. Mater.* **2015**, *3*, 280–320; b) Y. Patil, R. Misra, M. K. Singh, G. D. Sharma, *Phys. Chem. Chem. Phys.* **2017**, *19*, 7262–7269; c) Y. Patil, R. Misra, F.-C. Chen, G. D., *Phys. Chem. Chem. Phys.* **2016**, *18*, 22999–23005; d) Y. Patil, J. Shinde, R. Misra, *J. Organomet. Chem.* **2017**, *852*, 48–53.
[42] a) Y. Patil, R. Misra, F.-C. Chen, M. L. Keshtov, G. D. Sharma, *RSC Adv.* **2016**, *6*, 99685–99694; b) C. Popli, Y.

Jang, Y. Patil, R. Misra, F. D'Souza, *Chem. Eur. J.* **2020**, *26*, 15109; c) C. Popli, Y. Patil, R. Misra, *Eur. J. Org. Chem.* **2018**, *2018*, 6474–6481.
[43] a) Y. Patil, R. Misra, M. L. Keshtov, G. D. Sharma, *J. Phys. Chem. C* **2016**, *120*, 6324–6335; b) Y. Patil, T. Jadhav, B. Dhokale, R. Misra, *Eur. J. Org. Chem.* **2016**, *4*, 733–738; c) Y. Patil, T. Jadhav, B. Dhokale, R. Misra, *Asian J. Org. Chem.* **2016**, *5*, 1008–1014.
[44] a) T. Yamagata, J. Kuwabara, T. Kanbara, *Eur. J. Org. Chem.* **2012**, 5282–5290; b) E. Heyer, R. Ziessel, *Synlett.* **2015**, *26*, 2109–2116.
[45] a) A. Tang, C. Zhan, J. Yao, E. Zhou, *Adv. Mater.* **2017**, *29*, 1600013; b) Y. Patil, C. Popli, R. Misra, *New J. Chem.* **2018**, *42*, 3892–3899.
[46] F. Khan, Y. Jang, Y. Patil, R. Misra, F. D'Souza, *Angew. Chem. Int. Ed.* **2021**, *60*, 20518–20527.
[47] a) J. Mei, K. R. Graham, R. Stalder, J. R. Reynolds, *Org. Lett.* **2010**, *12*, 660–663; b) E. Wang, W. Mammo, M. R. Andersson, *Adv. Mater.* **2014**, *26*, 1801–1826.
[48] X. K. Wee, W. K. Yeo, B. Zhang, V. B. C. Tan, K. M. Lim, T. E. Tay, M.-L. Go, *Bioorg. Med. Chem.* **2009**, *17*, 7562–7571.
[49] J.-L. Li, J.-J. Cao, L.-L. Duan, H.-L. Zhang, *Asian J. Org. Chem.* **2018**, *7*, 2147–2160.
[50] N. M. Randell, T. L. Kelly, *Chem. Rec.* **2019**, *19*, 973–988.
[51] Y. Rout, V. Chauhan, R. Misra, *J. Org. Chem.* **2020**, *85*, 4611–4618.
[52] a) A. S. Hart, B. K. C. Chandra, N. K. Subbaiyan, P. A. Karr, F. D'Souza, *ACS Appl. Mater. Interfaces* **2012**, *4*, 5813–5820; b) M.-J. Kim, Y.-J. Yu, J.-H. Kim, Y.-S. Jung, K.-Y. Kay, S.-B. Ko, C.-R. Lee, I.-H. Jang, Y.-U. Kwon, N.-G. Park, *Dyes Pigm.* **2012**, *95*, 134–141.
[53] Y. J. Chang, P.-T. Chou, Y.-Z. Lin, M. Watanabe, C.-J. Yang, T.-M. Chin, T. J. Chow, *J. Mater. Chem.* **2012**, *22*, 21704–21712.
[54] a) Y. Hua, S. Chang, D. Huang, X. Zhou, X. Zhu, J. Zhao, T. Chen, W.-K. Wong, W.-Y. Wong, *Chem. Mater.* **2013**, *25*, 2146–2153; b) A. Baheti, K. R. J. Thomas, C.-T. Li, C.-P. Lee, K.-C. Ho, *ACS Appl. Mater. Interfaces* **2015**, *7*, 2249–2262.
[55] a) G. D. Sharma, M. A. Reddy, D. V. Ramana, M. Chandrasekharam, *RSC Adv.* **2014**, *4*, 33279–33285; b) Q. Tan, X. Yang, M. Cheng, H. Wang, X. Wang, L. Sun, *J. Phys. Chem. C* **2014**, *118*, 16851–16855.
[56] a) Y. Rout, P. Gautam, R. Misra, *J. Org. Chem.* **2017**, *82*, 6840–6845; b) M. Poddar, R. Misra, *Chem. Asian J.* **2017**, *12*, 2908–2915.
[57] a) P. Didier, G. Ulrich, Y. Mely, R. Ziessel, *Org. Biomol. Chem.* **2009**, *7*, 3639–3642; b) S. Atilgan, T. Ozdemir, E. U. Akkaya, *Org. Lett.* **2010**, *12*, 4792–4795; c) T. Rousseau, A. Cravino, E. Ripaud, P. Leriche, S. Rihn, A. De Nicola, R. Ziessel, J. Roncali, *Chem. Commun.* **2010**, *46*, 5082–5084.
[58] a) S. L. Niu, C. Massif, G. Ulrich, R. Ziessel, P.-Y. Renard, A. Romieu, *Org. Biomol. Chem.* **2011**, *9*, 66–69; b) H. He, P.-C. Lo, S.-L. Yeung, W.-P. Fong, D. K. P. Ng, *Chem. Commun.* **2011**, *47*, 4748–4750; c) M. Tasior, J. Murtagh, D. O. Frimannsson, S. O. McDonnell, D. F. O'Shea, *Org. Biomol. Chem.* **2010**, *8*, 522–525.
[59] a) O. A. Bozdemir, R. Guliyev, O. Buyukcakir, S. Selcuk, S. Kolemen, G. Gulseren, T. Nalbantoglu, H. Boyaci, E. U. Akkaya, *J. Am. Chem. Soc.* **2010**, *132*, 8029–8036; b) S. Atilgan, T. Ozdemir, E. U. Akkaya, *Org. Lett.* **2008**, *10*, 4065–4067.
[60] a) S. Erten-Ela, M. D. Yilmaz, B. Icli, Y. Dede, S. Icli, E. U. Akkaya, *Org. Lett.* **2008**, *10*, 3299–3302; b) S. Kolemen, Y. Cakmak, S. Erten-Ela, Y. Altay, J. Brendel, M. Thelakkat, E. U. Akkaya, *Org. Lett.* **2010**, *12*, 3812–3815.
[61] a) T. Rousseau, A. Cravino, J. Roncali, T. Bura, G. Ulrich, R. Ziessel, *Chem. Commun.* **2009**, 1673–1675; b) T. Rousseau, A. Cravino, J. Roncali, T. Bura, G. Ulrich, R. Ziessel, *J. Mater. Chem.* **2009**, *16*, 2298–2300; c) B. Kim, B. Ma, V. R. Donuru, H. Liu, J. M. J. Frechet, *Chem. Commun.* **2010**, *46*, 4148–4150.
[62] a) B. Dhokale, T. Jadhav, S. M. M. R. Misra, *Dalton Trans.* **2016**, *45*, 1476–1483; b) M. Poddar, Y. Jang, R. Misra, F. D'Souza, *Chem. Eur. J.* **2020**, *26*, 6869–6878.
[63] a) P. Gautam, R. Misra, M. B. Thomas, F. D'Souza, *Chem. Eur. J.* **2017**, *23*, 9192; b) S. Niu, G. Ulrich, P. Retailleau, R. Ziessel, *Tetrahedron Lett.* **2011**, *52*, 4848–4853.
[64] a) G. Ulrich, A. Barsella, A. Boeglin, S. Niu, R. Ziessel, *ChemPhysChem* **2014**, *15*, 2693–2700; b) N. Songlin, G. Ulrich, P. Retailleau, R. Ziessel, *Org. Lett.* **2011**, *13*, 4996–4999.
[65] D. Pinjari, A. Z. Alsaleh, Y. Patil, R. Misra, F. D'Souza, *Angew. Chem. Int. Ed.* **2020**, *59*, 23697–23705; *Angew. Chem.* **2020**, *132*, 23905–23913.
[66] J. Du, M. C. Biewera, M. C. Stefan, *J. Mater. Chem. A* **2016**, *4*, 15771–15787.
[67] R. Misra, P. Gautam, *Org. Biomol. Chem.* **2014**, *12*, 5448–5457.
[68] Y. Rout, S. M. Mobin, R. Misra, *New J. Chem.* **2019**, *43*, 12299–12307.
[69] a) Y. O. Lee, T. Pradhan, S. Yoo, T. H. Kim, J. Kim, J. S. Kim, *J. Org. Chem.* **2012**, *77*, 11007; b) T. M. Figueira-Duarte, K. Mullen, *Chem. Rev.* **2011**, *111*, 7260–7314.
[70] C. Lambert, J. Ehbets, D. Rausch, M. Steeger, *J. Org. Chem.* **2012**, *77*, 6147–6154.
[71] B. Dhokale, T. Jadhav, S. M. Mobin, R. Misra, *RSC Adv.* **2015**, *5*, 57692–57699.
[72] a) N. N. P. Moonen, W. C. Pomerantz, R. Gist, C. Boudon, J. P. Gisselbrecht, T. Kawai, A. Kishioka, M. Gross, M. Irie, F. Diederich, *Chem. Eur. J.* **2005**, *11*, 3325–3341; b) Y. Lin, H. Fan, Y. Li, X. Zhan, *Adv. Mater.* **2012**, *24*, 3087–3106.
[73] R. Maragani, P. Gautam, R. Misra, *Tetrahedron Lett.* **2015**, *56*, 1664–1666.
[74] R. Maragani, S. Bijesh, R. Sharma, R. Misra, *Asian J. Org. Chem.* **2017**, *6*, 1408–1414.
[75] a) F. C. Krebs, N. Espinosa, M. Hösel, R. R. Søndergaard, M. Jørgensen, *Adv. Mater.* **2014**, *26*, 29–39; b) G. Li, R. Zhu, Y. Yang, *Nat. Photonics* **2012**, *6*, 153–161.
[76] a) A. Mishra, P. Bäuerle, *Angew. Chem. Int. Ed.* **2012**, *51*, 2020–2067; *Angew. Chem.* **2012**, *124*, 2060–2109; b) W. Ni, X. Wan, M. Li, Y. Wang, Y. Chen, *Chem. Commun.* **2015**,

51, 4936–4950; c) H. Yao, L. Ye, H. Zhang, S. Li, S. Zhang, J. Hou, *Chem. Rev.* **2016**, *116*, 7397–7457.
[77] a) L. Dou, J. You, Z. Hong, Z. Xu, G. Li, R. A. Street, Y. Yang, *Adv. Mater.* **2013**, *25*, 6642–6671; b) L. Lu, T. Zheng, Q. Wu, A. M. Schneider, D. Zhao, L. Yu, *Chem. Rev.* **2015**, *115*, 12666–12731.
[78] S. Shalini, R. Balasundara Prabhu, S. Prasanna, T. K. Mallick, S. Senthilarasu, *Renewable Sustainable Energy Rev.* **2015**, *51*, 1306–1325.
[79] O'Regan, M. Grätzel, *Nature* **1991**, *353*, 737–740.
[80] R. Misra, R. Maragani, K. R. Patel, G. D. Sharma, *RSC Adv.* **2014**, *4*, 34904–34911.
[81] A. Leliège, P. Blanchard, T. Rousseau, J. Roncali, *Org. Lett.* **2011**, *13*, 3098–3101.
[82] P. Gautam, R. Misra, E. N. Koukaras, A. Sharma, G. D. Sharma, *Org. Electron.* **2015**, *27*, 72–83.
[83] P. Gautam, R. Misra, G. D. Sharma, *Phys. Chem. Chem. Phys.* **2016**, *18*, 7235–7241.
[84] P. Gautam, R. Misra, S. A. Siddiqui, G. D. Sharma, *ACS Appl. Mater. Interfaces* **2015**, *7*, 10283–10292.
[85] P. Simón Marqués, J. M. A. Castán, B. A. L. Raul, G. Londi, I. Ramirez, M. S. Pshenichnikov, D. Beljonne, K. Walzer, M. Blais, M. Allain, C. Cabanetos, P. Blanchard, *Chem. Eur. J.* **2020**, *26*, 16422.
[86] a) G. Yu, J. Gao, J. C. Hummelen, F. Wudl, A. J. Heeger, *Science* **1995**, *270*, 1789–1791; b) N. S. Sariciftci, L. Smilowitz, A. J. Heeger, F. Wudl, *Science* **1992**, *258*, 1474–1476; c) Y. He, Y. Li, *Phys. Chem. Chem. Phys.* **2011**, *13*, 1970–1983.
[87] a) Y. Liu, C.-C. Chen, Z. Hong, J. Gao, Y. Yang, H. Zhou, L. Dou, G. Li, Y. Yang, *Sci. Rep.* **2013**, *3*, 3356–3363; b) B. Kan, M. Li, Q. Zhang, F. Liu, X. Wan, Y. Wang, W. Ni, G. Long, X. Yang, H. Feng, *J. Am. Chem. Soc.* **2015**, *137*, 3886–3893.
[88] a) Q. Zhang, B. Kan, F. Liu, G. Long, X. Wan, X. Chen, Y. Zuo, W. Ni, H. Zhang, M. Li, *Nat. Photonics* **2015**, *9*, 35–41; b) K. Sun, Z. Xiao, S. Lu, W. Zajaczkowski, W. Pisula, E. Hanssen, J. M. White, R. M. Williamson, J. Subbiah, J. Ouyang, *Nat. Commun.* **2015**, *6*, 6013–6021.
[89] a) W. Zhao, S. Li, H. Yao, S. Zhang, Y. Zhang, B. Yang, J. Hou, *J. Am. Chem. Soc.* **2017**, *139*, 7148–7151; b) K. M. Coakley, M. D. McGehee, *Chem. Mater.* **2004**, *16*, 4533–4542; c) W. Huang, M. Li, L. Zhang, T. Yang, Z. Zhang, H. Zeng, X. Zhang, L. Dang, Y. Liang, *Chem. Mater.* **2016**, *28*, 5887–5895.
[90] a) Y. Zang, C.-Z. Li, C.-C. Chueh, S. T. Williams, W. Jiang, Z.-H. Wang, J.-S. Yu, A. K.-Y. Jen, *Adv. Mater.* **2014**, *26*, 5708–5714; b) A. D. Hendsbee, J.-P. Sun, W. K. Law, H. Yan, I. G. Hill, D. M. Spasyuk, G. C. Welch, *Chem. Mater.* **2016**, *28*, 7098–710917.
[91] T. Shoji, S. Ito, *Chem. Eur. J.* **2017**, *23*, 16696–16709.
[92] Y. Patil, R. Misra, R. Singhal, G. D. Sharma, *J. Mater. Chem. A* **2017**, *5*, 13625–13633.
[93] Y. Patil, R. Misra, M. L. Keshtov, G. D. Sharma, *J. Mater. Chem. A* **2017**, *5*, 3311–3319.
[94] A. A. Raheem, C. Kumar, P. Murugan, C. Praveen, *ACS Appl. Energ. Mater.* **2021**, *4*, 11609–11623.
[95] A. A. Raheem, P. Murugan, R. Shanmugam, C. Praveen, *ChemPlusChem.* **2021**, *86*, 1451.
[96] a) J. Wang, R. Yan, F. Guo, M. Yu, F. Tan, N. Li, *Nanotechnology* **2016**, *27*, 285102; b) M. Sun, F. Liu, Y. Zhu, W. Wang, J. Hu, J. Liu, Z. Dai, K. Wang, Y. Wei, J. Bai, *Nanoscale* **2016**, *8*, 4452–4457.
[97] a) P. Huang, Y. Gao, J. Lin, H. Hu, H.-S. Liao, X. Yan, Y. Tang, A. Jin, J. Song, G. Niu, *ACS Nano* **2015**, *9*, 9517–9527; b) P. Huang, J. Lin, W. Li, P. Rong, Z. Wang, S. Wang, X. Wang, X. Sun, M. Aronova, G. Niu, R. D. Leapman, Z. Nie, X. Chen, *Angew. Chem. Int. Ed.* **2013**, *125*, 14208–14214.
[98] a) P. Liang, Y. Wang, P. Wang, J. Zou, H. Xu, Y. Zhang, W. Si, X. Dong, *Nanoscale* **2017**, *9*, 18890–18896; b) Y. Cai, P. Liang, Q. Tang, X. Yang, W. Si, W. Huang, Q. Zhang, X. Dong, *ACS Nano* **2017**, *11*, 1054.
[99] Y. Cai, P. Liang, W. Si, B. Zhao, J. Shao, W. Huang, Y. Zhang, Q. Zhang, X. Dong, *Org. Chem. Front.* **2018**, *5*, 98–105.
[100] C. Ornelas, *New J. Chem.* **2011**, *35*, 1973–1985.
[101] S. Ghosh, T. Avellini, A. Petrelli, I. Kriegel, R. Gaspari, G. Almeida, G. Bertoni, A. Cavalli, F. Scotognella, T. Pellegrino, *Chem. Mater.* **2016**, *28*, 4848–4858.

Manuscript received: August 17, 2022
Revised manuscript received: September 9, 2022
Version of record online: October 6, 2022

